Frequency range optimization for linear viscoelastic characterization of Burger's model

Wang, Chen; Anupam, Kumar; Kasbergen, Cor; Erkens, Sandra

DOI
10.1016/j.ijmecsci.2024.109817

Publication date
2024

Document Version
Final published version

Published in
International Journal of Mechanical Sciences

International Journal of Mechanical Sciences 285 (2025) 109817

Contents lists available at ScienceDirect

International Journal of Mechanical Sciences

journal homepage: www.elsevier.com/locate/ijmecsci

Frequency range optimization for linear viscoelastic characterization of Burger's model

Chen Wang, Kumar Anupam *, Cor Kasbergen, Sandra Erkens

Section of Pavement Engineering, Faculty of Civil Engineering & Geosciences, Delft University of Technology, Stevinweg 1, 2628 CN Delft, the Netherlands

ARTICLE INFO

Keywords:
Viscoelastic characterization
Constitutive modeling
Computational method
Burger's model
Optimal frequency range
Stress relaxation

ABSTRACT

The linear viscoelastic behavior of materials is represented using mechanical models of choice, which are further utilized in different numerical investigations, such as finite element simulations and discrete element simulations. Burger's model is one of the widely adopted mechanical models and remains highly favored in contemporary research due to its multiple advantages. Specifically, it excels in representing long-term creep and stress relaxation behavior in a relatively simplified manner. Accurate identification of the long-term behavior for the viscoelastic material, particularly asphalt concrete, is crucial, as it serves as a key indicator of asphalt pavement performance over its service life. However, past research studies show that the parameters of Burger's model should be back-calculated from experimental data only within a limited range of frequency, otherwise, the parameters fail to represent the true material behavior. To the best of the authors' knowledge, there is no approach for researchers to obtain the critical frequency range in which the experiments should be performed. Therefore, this study proposes a novel framework to find the critical frequency range to obtain appropriate model parameters of Burger's model, to better characterize the viscoelastic behavior of the materials. To examine the framework, asphalt concrete mixtures are used as examples in this study. Necessary laboratory tests including complex modulus tests and stress relaxation tests, are performed on two distinctive types of asphalt concrete mixtures. The generalized Maxwell model with different number of Maxwell chains are used to evaluate the performance of Burger's model. Furthermore, since commercially available finite element packages generally do not have a direct built-in Burger's model, the article shows a way of implementing Burger's model in finite element simulation. The simulations corresponding to the laboratory tests are carried out in both frequency domain and time domain to thoroughly evaluate the performance of Burger's model. The optimal frequency range of 0.1–20 Hz for the examined mixtures is found to significantly improve the accuracy of the descriptive master curve. The results also suggest that the generalized Maxwell model requires a minimum of four Maxwell chains to maintain good performance in accurately characterizing the behavior of asphalt mixtures. However, adding more Maxwell chains beyond a critical limit may not provide significant benefits. Finite element simulations demonstrate that the stress relaxation behavior predicted by the obtained Burger's model parameters aligns more closely with experimental data over longer time intervals. This makes Burger's model a strong choice for aiding in the design of simulations for studies focused on the long-term behavior of materials.

1. Introduction

Viscoelasticity becomes an important aspect in modelling dynamic responses of many flexible multibody systems [1]. Hence, an accurate representation of the viscoelastic bodies in concern is of prime importance in many disciplines. Asphalt concrete (AC) is typically considered as a viscoelastic material that consists of aggregate particles, bitumen, fines, and sometimes other additives [2]. The inclusion of various types of constituent materials results in different viscoelastic behaviour. The design of the pavement and its life-time performance is directly related to the rheological properties which describe the time-dependent (viscoelastic) behaviour of materials [3,4]. Hence, the reliable prediction of the performance can only be achieved if the appropriate assessment of rheological properties is incorporated into the performance prediction toolkit [5]. The accurate characterization of viscoelastic behaviour in the prediction tool serves as an important task for pavement asset management.

The viscoelastic behaviour possesses linear and nonlinear

* Corresponding author.
E-mail address: k.anupam@tudelft.nl (K. Anupam).

https://doi.org/10.1016/j.ijmecsci.2024.109817
Received 24 April 2024; Received in revised form 28 October 2024; Accepted 5 November 2024
Available online 9 November 2024

characteristics depending on the selection of materials and load applications [6]. To assess the nonlinear viscoelastic properties, complicated mathematical formulations are required [7,8], whereas the linear viscoelastic description is relatively straightforward. Therefore, in the laboratory, usually small strain level (typically < 100 μm/m) [9] tests are performed and linear viscoelastic (LVE) characteristics (such as dynamic modulus) are used as a key parameter for the prediction of field performance of the material [10]. Over the years, researchers have developed different procedures [11–17] to characterize LVE properties of materials. The common principle underlying these procedures involves laboratory tests in either the time domain (creep and relaxation tests) or in the frequency domain (complex modulus/DMA tests). The major difference among their LVE characterization procedures is reflected in the utilization of different mechanical models [18–23].

Mechanical or mathematical models describe viscoelastic behaviour by using a constitutive relationship that accounts for the material's response based on factors such as stress/strain levels, loading rates, and stress states [24,25]. Among different mechanical models, the stress-strain relationships are often expressed using combinations of linear springs (Hooke's element) and dashpots (Newton's element). This gives mechanical models the advantage of providing a physical interpretation for each parameter [26], unlike several empirical models [27, 28], which are primarily based on statistical relationships. Moreover, mechanical models have become popular due to the widespread adoption of computational methods, such as the Finite Element Method (FEM) [29–31] and the Discrete Element Method (DEM) [32–34]. However, it should be noted that different mechanical models can be accurate or inaccurate depending upon the conditions of applications [18]. A brief review of widely used mechanical models is given in the subsequent paragraphs.

Researchers [32,35,36] have evaluated the capability of different mechanical models consisting of 2–4 spring/dashpots, for characterizing the LVE behavior of different viscoelastic materials. Feng [32] revealed the limitations of two-element models (e.g., Maxwell model or Kelvin-Voigt model), noting that these models cannot accurately describe the LVE behavior under both imposed stress and imposed strain conditions. Furthermore, Hubert [35] highlighted that four-element models (Burger's model) can accurately represent rheological behavior (creep compliance) of polymethyl methacrylate without compromising fitting accuracy, deeming it the best option for modelling the viscoelastic behavior of resists for nanoimprint lithography. Similarly, Arindam [36] concluded that Burger's model has the excellent potential for correctly representing the time-dependent behavior of viscoelastic soils beds.

Mechanical models with more than four elements, such as the generalized Maxwell (GM) model and the generalized Kelvin-Voigt (GKV) model, are frequently used to characterize the LVE behavior of the materials. Kim et al. [37,38] employed the GM model, represented through Prony series coefficients [39], to characterize the viscoelastic properties in the time domain within their performance prediction model. Duffrène [40] employed the GM model to characterize the multiaxial linear viscoelastic behavior of a soda–lime–silica glass using creep-recovery tests.

In addition to the models comprised of a simple combination of linear springs and dashpots, an alternative approach to modelling viscoelastic response involves the use of a parabolic element [41,42]. This element governs the viscoelastic response of materials by introducing a differential equation of a non-integer order [43], while the simple spring and dashpot only formulate the response function in an integer order. This unique expression, also known as fractional derivative [21,44], can be used to represent an infinite number of Maxwell or Kelvin-Voigt elements. Representative models [45,46] that incorporate the parabolic elements, such as the 2S2P1D model, have been reported to accurately characterize the LVE behavior of different types of viscoelastic materials. However, it is noted that the numerical implementation of fractional derivative models is far more complicated than models composed of simple spring and dashpot. The development of numerical simulation for fractional derivative models falls outside the scope of this research.

Generally, the use of spring or dashpot element-based models often leads to a suboptimal fitting of the master curve, as compared to fractional derivative models. Researchers [26] have reported that an apparent "waveform" is particularly pronounced in models with fewer discrete spectrums. The GM/GKV model, as a representative of these models, also exhibits this limitation. However, incorporating an increased number of Maxwell/Kelvin chains spans the applicable frequency range with more flexibility in defining viscosity effects. Consequently, the GM/GKV model remains effective across the wide range of frequencies for the LVE characterization. In addition, GM model's constitutive formulation yields the Prony series representation [47], provides a straightforward way for implementation in the computational method. This approach is particularly favoured in finite element simulations of asphalt mixtures, where the Prony series model has become one of the most widely adopted choices [48–52]. This type of LVE representation has been available in finite element software, such as Abaqus [53], MSC Marc [54] and ANSYS [55]. However, researchers [41,56] emphasized that GM/GKV models usually require a considerable number of Maxwell or Kelvin-Voigt chains to achieve a satisfactory curve fitting. Olard [41] noted a minimum of eight Maxwell elements is required for the GM model, while Milliyon [56] concluded that a minimum of 10 to 15 Kelvin-Voigt elements (equivalent to 21 to 31 model parameters) is needed for the GKV model. It is noted that adopting a higher number of parameters may lead to statistical underfitting and unreliable results [57]. Additionally, determining these parameters can present a mathematically ill-posed problem [58]. Furthermore, excessive model parameters can reduce computational efficiency, which is crucial as contemporary studies often require increasingly complex simulations and longer computational times [59]. Therefore, evaluating the performance of the Prony series (GM) model with different numbers of Maxwell chains is a valuable analysis for balancing accuracy and computational efficiency.

Burger's model has been prominently used and remains favoured in various studies over the past decades [36,60–66]. In certain applications, such as DEM simulations [67,68] of asphalt mixtures, Burger's model is the most widely adopted choice among other models. This is because of its numerous advantages. Burger's model is the simplest model that incorporates both Maxwell and Kelvin-Voigt elements, allowing it to represent both creep and stress relaxation behavior in the time domain (long-term behaviour) [66]. In addition, the Maxwell and Kevin-Voigt element in series allow Burger's model to describe the elastic, viscous and viscoelastic components of material response. In particular, the viscous component of the material response reflects the remaining part of the material deformation, which is shown to be a characteristic feature observed in asphalt mixtures. Researchers [69–72] have highlighted that other models, built on the foundations of the generalized Maxwell and Kelvin model, can also improve long-term predictions in finite element and discrete element simulations. The reasoning is similar to that of Burger's model, as these models incorporate at least one Maxwell and one Kelvin-Voigt element. However, assessing these models requires significantly more effort in mathematical derivation and numerical implementation than Burger's model, which is beyond the scope of this paper.

Typically, above advantages of Burger's model are not fully captured by assessing the fitted master curve in the frequency domain, which is the common method of evaluation. However, contemporary research increasingly focuses on evaluating time-domain behavior, such as stress recovery and stress relaxation, which are more relevant to practical applications [73]. The ability of Burger's model to perform well in these time-domain analyses contributes to its continued popularity. Moreover, for Burger's model, the use of four model parameters can reduce the computational time for the numerical simulation. However, Burger's model exhibits the drawback in its poor fitting for the master curve, due

to the presence of the "waveform" behavior [26]. As a result, the accuracy in simulating the LVE behavior in the computational method can be influenced. This is because the implementation of the mechanical models for the numerical simulation generally follows the so-called back-calculation technique, where the FEM or DEM input parameters are back-calculated through the fitting of the master curve in the frequency domain. In addition, such "waveform" behavior makes the back-calculated Burger's model parameters sensitive to the frequency range of complex modulus data. The utilization of different frequency ranges causes variations in the obtained model parameters. Hence, the researchers [74–77] concluded that Burger's model accurately describes the linear viscoelastic behavior of the materials within a limited frequency range. To the best of the author's knowledge, limited research has focused on identifying this critical frequency range to obtain appropriate parameters of Burger's model. Given that Burger's model is often the preferred choice or serves as the foundation for most models in certain applications, such as DEM modelling, it is highly promising to propose an optimal frequency identification.

The structure this article is organized as follows: The research objective and scopes are outlined in the subsection (Section 1.1) of the introduction. Section 2 provides an overview of the methodology, detailing the proposed framework and its working procedure for identifying the optimal frequency range. Section 3 describes the laboratory tests conducted for the calibration and validation of the framework. In Section 4, the finite element simulation process is presented, including the modelling of laboratory tests and the derivation of the material subroutine. Section 5 presents the results, including the obtained optimal frequency range for the examined materials and performance evaluation of the proposed framework. Finally, Section 6 summarizes the conclusions and potential directions for future research. Additional details, such as laboratory test information and the derivation of equations for the material model, are presented in the Supplementary material.

1.1. Research objective and scopes

The present article proposes a framework capable of providing an optimal frequency range to obtain better model parameters for Burger's model. This framework is expected to be a valuable tool for practitioners and researchers who would like to adopt Burger's model for their (FEM, DEM, etc.) numerical investigations. Since the proposed approach utilizes simple statistical assessments, it can also be used to judge the relative performance of different models. Keeping the above in mind, the following research scopes were identified:

- Propose a simple statistics-based framework capable of identifying the optimal frequency range for Burger's model based on laboratory investigations.
- Demonstration of the working procedure of the proposed framework via two types of asphalt mixtures. One of the mixtures consisting of virgin materials, serves as the reference, while another type of mixture consisting of reclaimed asphalt pavement materials (RAP) and agent, represents the prevalent mixture type in the current practice.
- Performance evaluation of the proposed framework with both frequency domain and time domain data which are obtained from laboratory tests.
- Implementation of the FE model by incorporating material subroutines to further investigate the performance of the proposed framework.
- Comparison of the relative performances of Burger's model within the optimized frequency range and the GM model with different number of Maxwell chains (N = 2, 3, 4, 5, 6 and 13) using the tested frequency range.

2. Methodology

The methodology of this paper, as shown in Fig. 1, is discussed in the following sections. This section aims to provide a detailed description of the proposed framework to find the optimal frequency range for Burger's model. At first, a brief literature overview of GM and Burger's model, including their relevant equations, is presented.

2.1. Brief overview of Burger's model and GM model

In this subsection, the necessary derivation for the constitutive equations is discussed. Burger's model is a four-element model incorporating a Maxwell element and a Kelvin-Voigt element (see Fig. 2(a)). The constitutive equation of Burger's model can be expressed in a differential form, as shown in Eq. (1):

$$\sigma + p_1\dot{\sigma} + p_2\ddot{\sigma} = q_1\dot{\varepsilon} + q_2\ddot{\varepsilon}, \tag{1}$$

where p_1, p_2, q_1 and q_2 are constants of Burger's model in the differential operator and each constant can be described in terms of four model parameters in Fig. 2(a), as shown in Eq. (2)-(5):

$$p_1 = \frac{\eta_m}{E_m} + \frac{\eta_m}{E_k} + \frac{\eta_k}{E_k}, \tag{2}$$

$$p_2 = \frac{\eta_m\eta_k}{E_mE_k}, \tag{3}$$

$$q_1 = \eta_m, \tag{4}$$

$$q_2 = \frac{\eta_m\eta_k}{E_k}, \tag{5}$$

The time-domain LVE equation (creep compliance) of Burger's model was derived from Eq. (1), as shown in Eq. (6):

$$D(t) = \frac{1}{E_m} + \frac{t}{\eta_m} + \frac{1}{E_k}\left(1 - e^{-\frac{E_k}{\eta_k}t}\right), \tag{6}$$

where $D(t)$ represents the creep compliance of Burger's model.

The interconversion approaches [78] involving the Carson-Laplace transform (see Eq. (7)) were employed to convert the creep compliance from the time domain to a complex s ($s = i\omega$) domain, as shown in Eq. (8):

$$\widetilde{f}(s) = s\cdot\int_0^\infty f(t)e^{-st}dt, \tag{7}$$

$$\widetilde{D}(s) = s\cdot\left(\frac{1}{E_ms} + \frac{1}{\eta_ms^2} + \frac{1}{E_ks} - \frac{1}{E_k\left(s + \frac{E_k}{\eta_k}\right)}\right). \tag{8}$$

As the reciprocal of Eq. (8), the complex modulus of Burger's model was obtained, as shown in Eq. (9).

$$E^*(i\omega) = \widetilde{E}(s)|_{s\to i\omega} = \frac{1}{\widetilde{D}(s)} = \frac{i\omega E_m\eta_mE_k - \omega^2E_m\eta_m\eta_k}{-\eta_m\eta_k\omega^2 + \omega[i\eta_m(E_m+E_k) + iE_m\eta_k] + E_mE_k}, \tag{9}$$

where ω is the angular frequency.

The storage modulus and loss modulus of Burger's model were obtained by calculating the real and the imaginary part of Eq. (9):

$$E'(\omega) = \frac{E_m{\eta_m}^2({\eta_k}^2\omega^2 + E_k(E_k+E_m))\omega^2}{{\eta_k}^2{\eta_m}^2\omega^4 + \left((\eta_k+\eta_m)^2{E_m}^2 + 2E_k{\eta_m}^2E_m + {E_k}^2{\eta_m}^2\right)\omega^2 + {E_m}^2{E_k}^2}, \tag{10}$$

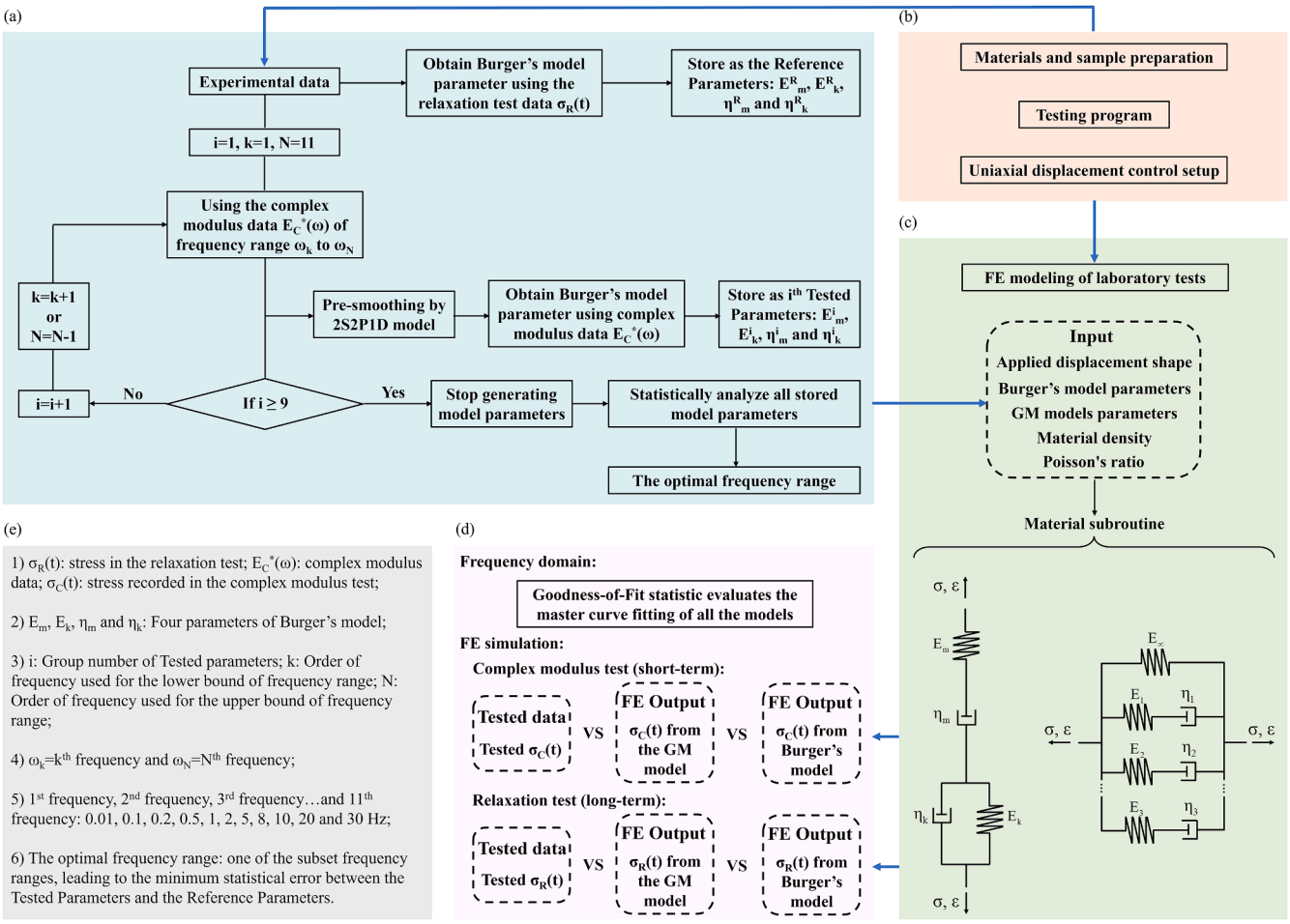

Fig. 1. Overview of research methodology: (a) Proposed framework for determining the optimal frequency range for Burger's model. This subfigure illustrates the process of identifying the optimal frequency subset range, utilizing experimental data from both complex modulus and relaxation tests. Model parameters derived from the relaxation test data serve as reference values, guiding the evaluation of model parameters obtained from complex modulus test data across different subset frequency ranges. Number k and N dictate the frequency data point limits, generating various subset frequency ranges for evaluation. Statistical analysis of all derived model parameters ultimately determines the optimal frequency range. (b) Laboratory tests. Complex modulus and relaxation test data are used as inputs for the proposed framework, while asphalt sample geometry and test conditions inform the FE simulation. (c) FE simulation process. Model parameters from the identified optimal frequency range are the key input to define the material's linear viscoelastic properties. Two material model subroutines are implemented within the FE software. (d) Performance evaluation of Burger's Model in both frequency and time domains, comparing FE simulation results with test results. (e) Nomenclature and additional explanations related to terms and processes in the methodology.

$$E''(\omega)=\frac{{E_m}^2\eta_m\left(\eta_k(\eta_k+\eta_m)\omega^2+{E_k}^2\right)\omega}{{\eta_k}^2{\eta_m}^2\omega^4+\left((E_k+E_m)^2{\eta_m}^2+2\eta_k{E_m}^2\eta_m+{\eta_k}^2{E_m}^2\right)\omega^2+{E_m}^2{E_k}^2}. \tag{11}$$

Therefore, the LVE function of Burger's model in the frequency domain was obtained. In addition, the relaxation modulus of Burger's model was also adopted in this study. Using the four constants in Eq. (1), the relaxation modulus of Burger's model can be described in Eq. (12):

$$E(t)=\frac{1}{A}\left[(q_1-q_2r_1)e^{-r_1t}-(q_1-q_2r_2)e^{-r_2t}\right], \tag{12}$$

where $E(t)$ is the relaxation modulus of Burger's model, $A=\sqrt{{p_1}^2-4p_2}$, $r_1=(p_1-A)/2p_2$ and $r_2=(p_1+A)/2p_2$.

Eq. (10)-(12) are the kernel functions used in the proposed framework for this study.

The generalized Maxwell (GM) model consists of a linear spring and multiple Maxwell elements in parallel, as shown in Fig. 2(b).

The time domain LVE function under imposed strain (relaxation modulus) of the GM model is expressed using Eq. (13) [78]:

$$E(t)=E_\infty+\sum_{i=1}^{N}E_i e^{-\left(\frac{t}{\rho_i}\right)}, \tag{13}$$

The corresponding constitutive equations in the frequency domain can be found elsewhere [79], as shown in Eq. (14)-(15).

$$E'(\omega)=E_\infty+E_0\sum_{i=1}^{N}\frac{g_i{\rho_i}^2\omega^2}{1+{\rho_i}^2\omega^2}, \tag{14}$$

$$E''(\omega)=E_0\sum_{i=1}^{N}\frac{g_i\rho_i\omega}{1+{\rho_i}^2\omega^2}, \tag{15}$$

where E_0 is the instantaneous moduli of the viscoelastic material, g_i is the weight of relative modulus to the instantaneous moduli E_i/E_0. In these constitutive equations (see Eq. (13)-(15)) of GM model, N represents the number of the Maxwell chains, and GM model with $N=2$, 3, 4, 5, 6 and 13 were analysed in this study. It is noted that theoretically, the proposed approach allows for the evaluation of the relative performance of GM model with any values of N. However, for an illustrative purpose, a range of small N (from two to six) and an extreme case of $N=13$ (limit of several commercially available FE software, such as Abaqus) were

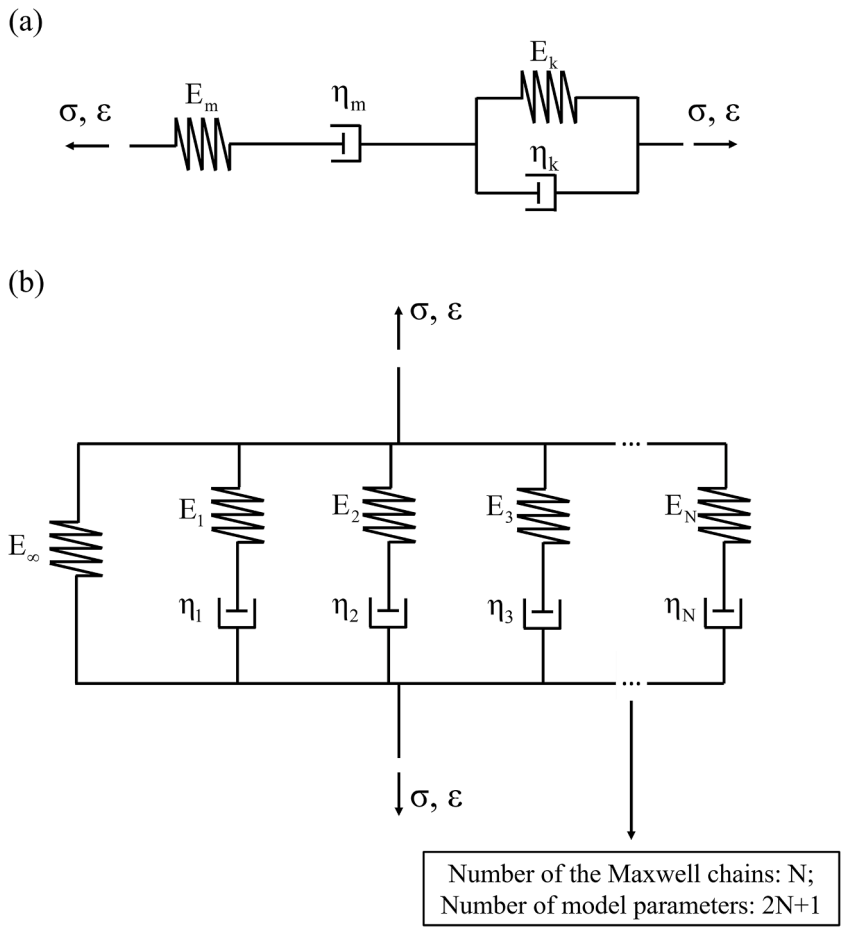

Fig. 2. Mechanical models considered in this study: (a) Burger's model, characterized by four parameters: E_m (elastic modulus of the Maxwell spring), η_m (viscosity of the Maxwell dashpot), E_k (Kelvin spring modulus), and η_k (Kelvin dashpot viscosity). (b) Generalized Maxwell model, where E_∞ represents the equilibrium moduli (in uniaxial direction) of viscoelastic material. For each Maxwell element, E_i is the relative Young's modulus for each Maxwell element, η_i is the viscosity, and $\rho_i=\eta_i/E_i$ represents the relaxation time. Consequently, for GM model with N Maxwell chains, the total number of model parameters is 2N+1.

selected.

2.2. Proposed framework to find the optimal frequency range for Burger's Model

As discussed in the introduction, the back-calculated Burger's model parameters are sensitive to the utilized frequency ranges, hence, going beyond the optimal frequency range may lead to an incorrect description of the LVE behavior. In such cases, it is necessary to incorporate a prior step in which the optimal frequency range is determined from the tested data. It is important to note that determining the optimal frequency range requires specifying a reference temperature to plot the master curve. Accordingly, the proposed framework is applicable at any reference temperature to identify the optimal frequency range and in this paper, a case study using a reference temperature of 10 °C was presented. It is possible that different temperatures could results in varying optimal frequency ranges. However, due to the length constraints and a focus on the working procedure of the framework in this article, the effect of temperature on the framework will be explored in future research.

To obtain the optimal frequency range using the proposed framework (see Fig. 1(a)), the sensitivity analysis of the back-calculated model parameters with respect to different frequency ranges (Fi) needs to be carried out. The optimal frequency range is selected from a group of subsets of tested frequencies via simple statistical investigation. The subset of frequency range was defined based on the need to explore the effect of reducing available frequency data points, while maintaining a sufficient number of data points for reliable analysis. First, these subsets of frequency ranges are generated by randomly removing the frequency data points from either the top or bottom of the experimental frequency range (see Fig. 1(a)). In addition, to ensure that the reduced frequency range would still be sufficient for meaningful LVE characterization, a lower limit was set to be half of the original data points (i.e., a minimum of 6 out of 11). Specifically, the subset frequency ranges were stopped to generate once the number of data points was reduced to six. Based on these criteria, the subsets ranges shown in the second column of Table 1 were generated, with no preference given to any specific frequency data points.

Among these defined subset ranges, the optimal subset frequency range is found based on statistical assessment for the obtained (Tested) back-calculated parameters (E_m^i, E_k^i, η_m^i and η_k^i) against the Reference back-calculated parameters (E_m^R, E_k^R, η_m^R and η_k^R). Therefore, the reference behavior should be a "true" (close) representation of the actual material behavior. For this purpose, this research employs relaxation test data ($\sigma_R(t)$) which is expected to capture the long-term behavior of viscoelastic material more accurately. Eq. (12) was used to obtain the back-calculated Reference parameters. In addition, as shown in Fig. 1(a), the pre-smoothing technique was introduced. A brief description is provided in the following subsection.

2.2.1. Pre-smoothing technique

Fig. 1(a) shows that a pre-smoothing technique based on the 2S2P1D model was implemented for obtaining the Tested Parameters (E_m^i, E_k^i, η_m^i and η_k^i). This technique is introduced in the framework to address the

Table 1
The generated subset frequency ranges and nomenclature.

i	Subset frequency ranges	Nomenclature	
		Subset frequency ranges Fi	Tested parameters
1	0.01, 0.1, 0.2, 0.5, 1, 2, 5, 8, 10, 20 and 30 Hz	F1	E_m^1, E_k^1, η_m^1 and η_k^1
2	0.01, 0.1, 0.2, 0.5, 1, 2, 5, 8, 10 and 20 Hz	F2	E_m^2, E_k^2, η_m^2 and η_k^2
3	0.01, 0.1, 0.2, 0.5, 1, 2, 5, 8, 10 and 30 Hz	F3	E_m^3, E_k^3, η_m^3 and η_k^3
4	0.1, 0.2, 0.5, 1, 2, 5, 8, 10, 20 and 30 Hz	F4	E_m^4, E_k^4, η_m^4 and η_k^4
5	0.01, 0.2, 0.5, 1, 2, 5, 8, 10, 20 and 30 Hz	F5	E_m^5, E_k^5, η_m^5 and η_k^5
6	0.1, 0.2, 0.5, 1, 2, 5, 8, 10 and 20 Hz	F6	E_m^6, E_k^6, η_m^6 and η_k^6
7	0.1, 0.2, 0.5, 1, 2, 5, 8, 10 Hz	F7	E_m^7, E_k^7, η_m^7 and η_k^7
8	0.2, 0.5, 1, 2, 5, 8, 10, 20 Hz	F8	E_m^8, E_k^8, η_m^8 and η_k^8
9	0.2, 0.5, 1, 2, 5, 8, 10 Hz	F9	E_m^9, E_k^9, η_m^9 and η_k^9

difficulties associated with complex modulus data, which often exhibit local variances or scatters [80]. Direct fitting of experimental data to the mechanical models, particularly the Prony series model used in this study, frequently leads to issues such as negative spectrum strengths and local spectrum oscillations [81]. The pre-smoothing technique provides a simple and practical approach to overcome these difficulties by generating a smoothed curve based on the experimental data. Over the years, this technique has been implemented using various broadband functions, such as simple power-law series [81], empirical algebraic models like sigmoidal functions, the Christensen-Anderson-Marasteanu (CAM) model, and the Havriliak-Negami model [82–84]. In addition, it has been applied with mechanical models, including the Huet-Sayegh (HS) model and the 2S2P1D model [80,85]. As discussed in the introduction, the 2S2P1D model, a representative of fractional derivative models, produces a smooth master curve in the frequency domain. This model-based technique was incorporated into the framework to aid in determining the parameters for both Burger's model and the Prony series model.

As shown in Fig. 3, the 2S2P1D model incorporates parabolic elements (A and B) in addition to the spring and dashpot elements. Parabolic elements are representative of an infinite number of Maxwell

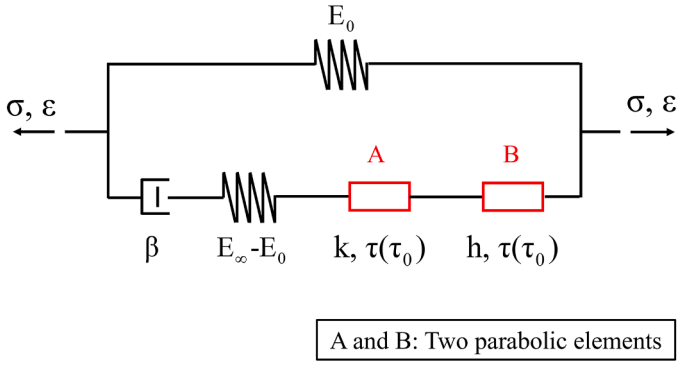

Fig. 3. 2S2P1D model. In this model, E_∞ represents the modulus at infinite frequency, and E_0 is the modulus at zero frequency. The viscosity of the single dashpot is denoted by β. Parameters h and k, where $1 > h > k > 1$, are the exponents for the two parabolic elements, A and B. The parameter $\tau(\tau_0)$, which is temperature-dependent, accounts for the Time-Temperature Superposition Principle. Additionally, the 2S2P1D model incorporates a parameter δ (not shown in the figure) to differentiate the fraction between the two parabolic elements, A and B.

elements or Kelvin-Voigt elements. The complex modulus in the 2S2P1D model is described in Eq. (16):

$$E^*(i\omega\tau) = E_0 + \frac{E_\infty - E_0}{1 + \delta(i\omega\tau)^{-k} + (i\omega\tau)^{-h} + (i\omega\beta\tau)^{-1}}, \quad (16)$$

Complex modulus $E_C^*(\omega)$ was at first fitted to the corresponding equation (see Eq. (16)). The curve fitting technique for the 2S2P1D model, as described in the literature [41], was used to obtain a smooth curve. Subsequently, the obtained smoothed curve was used to obtain the back-calculated parameters (E_m^i, E_k^i, η_m^i and η_k^i) with their corresponding frequency range (Fi), using Eq. (9)-(11).

2.2.2. Statistical evaluation

Once the parameters mentioned in the previous section were obtained, statistical evaluation was performed for all the Tested Parameters from each subset of the frequency range (Fi). For this purpose, three commonly used indicators namely: a) the standard error of the estimate (SEE), b) Root-Mean-Square Error (RMSE), and c) Mean Normalized Error (MNE) were used to measure the "statistical error" between the Tested Parameters and the Reference Parameters. The final decision of the optimal subset frequency range is obtained after consistent smallest values from all three errors are found.

2.2.3. Sample demonstration of the framework to obtain the optimal range

By following the described framework of Section 2.2.1, Table 1 was obtained based on conducted laboratory tests in this research (see Section 3). The second column of the corresponding table shows the different subsets of the frequency range that were generated. In order to have consistent results, the corresponding back-calculated (Tested) parameters are stored in different arrays (in accordance with the i value). All the data set that was generated in this last column was passed through statistical filtering, as described in Section 2.2.2. The results of statistical analysis and the determined optimal frequency range are shown in Section 5.1.

3. Description of laboratory tests

As explained in the previous section, the input data for the proposed framework were obtained through performing necessary laboratory tests in this research. Two different types of mixtures were considered to reduce any biased conclusions. This present section provides detailed information regarding the materials, samples, devices and methodological test programs. It is noted that the tests were conducted with standard devices that are used in pavement engineering with their prescribed norm EN 12,697–26.

3.1. Materials and sample preparation

In the present paper, two types of asphalt mixture samples, denoted as Mixture S1 and Mixture S2, were prepared (see Table 2), whereas a comprehensive breakdown of the studied mixtures is presented in the Supplementary material (see Section A1). Mixture S1 was produced with 100 % virgin aggregate, whereas Mixture S2 incorporated 70 % RAP (reclaimed asphalt pavement) material and 30 % virgin aggregate, with a recycling agent [86]. The produced mixtures were compacted using Superpave Gyratory Compactor. The compacted cylindrical specimens

Table 2
Description of the studied asphalt concrete mixtures.

Type of mixture	Description	Composition
S1	AC22 Base 40/60	100 %VA-0 %RAP (reference)
S2	AC22 Base 40/60 + 70 %PR & agent	30 %VA-70 %RAP + agent

were cored and polished to the desired size (100 mm in diameter and 150 mm in height) after storing them at 12 °C for a week.

3.2. Testing program

Fig. 4 shows all the laboratory tests that were performed on the cylindrical samples of Mixture S1 and Mixture S2. For both mixtures, two replicas were prepared to mitigate potential biases. Uniaxial displacement control tests were performed at two different loading modes. In the first loading mode, sinusoidal displacement was applied at different frequencies and temperatures to calculate the complex modulus, while in the second loading mode, the constant displacement was applied at same temperatures to calculate the relaxation modulus. To avoid non-LVE behavior, the resulting strain amplitude for both tests was kept low at 50 μm/m. After the relaxation test, a one-day recovery was adopted so that the samples could return to their initial state. To verify that the samples regained their initial strength, the complex modulus tests at 0.01 Hz, which were done before the relaxation test, were repeated after the recovery period. The data for complex modulus tests were recorded at the prescribed time interval Δt as shown Table 3. For the relaxation test, a constant time interval of 0.1 s was adopted.

3.3. Uniaxial displacement control setup

The uniaxial test setup for the complex modulus/relaxation tests can be seen in Fig. 5(a). The specimen was positioned between two plates of the diameter of 104±1 mm and the axial load was applied through the bottom plate. Three springs were arranged to create parallel lines, indicating the location of the Linear Variable Differential Transformer (LVDT) sensors at top and bottom. The measured difference in the movement between the bottom and top LVDT sensors reflects the displacement of the sample. These two displacement-control tests were performed by regulating the displacement to the desired form.

The sinusoidal displacement amplitude (for complex modulus tests) or constant displacement amplitude (for relaxation tests) was determined based on the geometries of the specimen, LVDT sensors, and the desired strain (50 μm/m) for both tests. A detailed geometry of the sample and setup can be found in the Supplementary material (see Section A2).

4. Finite element modeling to simulate the uniaxial displacement control setup

This section presents the implementation of viscoelastic models (Burger's model and GM model) for numerical simulations. In line with the objective of the research, these models were implemented inside the FE tool to gain a deeper understanding of the material responses under prescribed test conditions. Since many commercially available FE packages, such as Abaqus, ANSYS, and COMSOL Multiphysics [55,87], do not have a direct built-in Burger's model, a material subroutine was developed as part of this research. The outputs of the developed FE model were used to evaluate the performance of the Burger's model

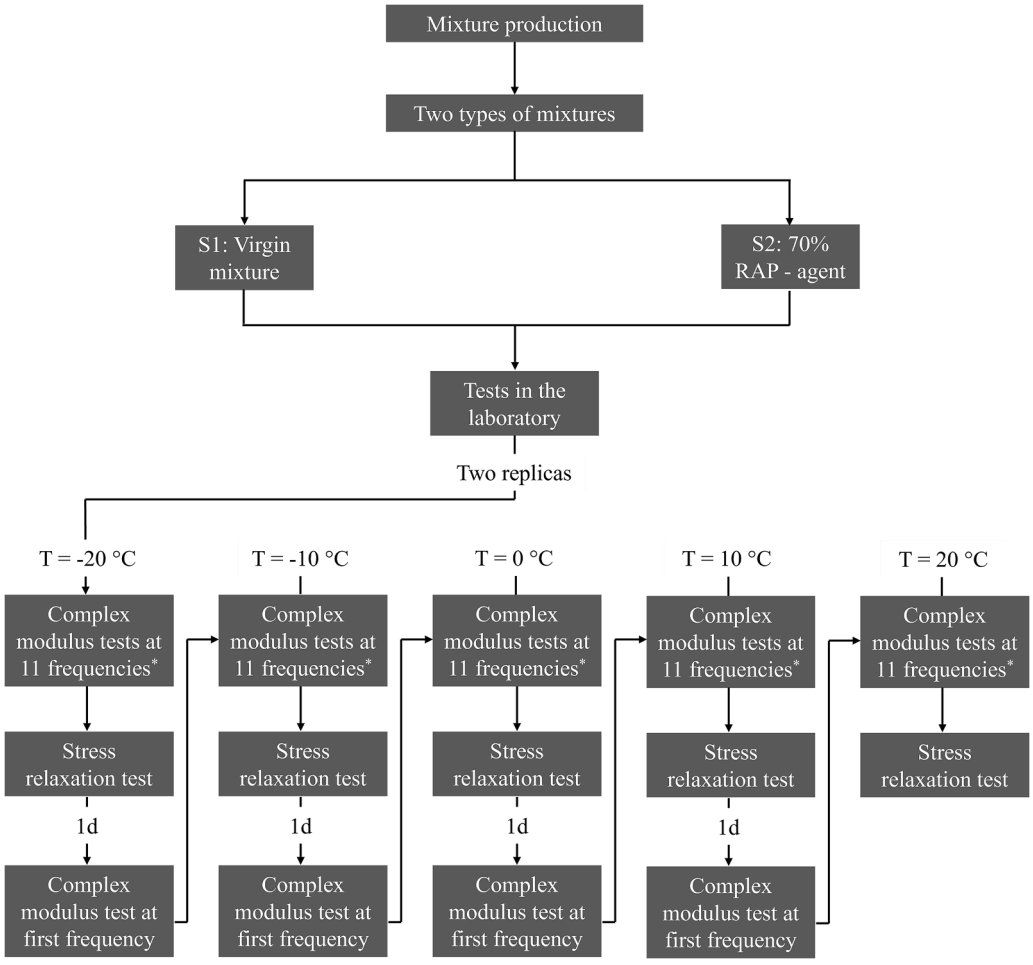

Fig. 4. Test program for displacement-control tests on two asphalt mixtures: Asphalt mixtures S1 (virgin mixture) and S2 (incorporating RAP materials and rejuvenating agent) are tested, with each test performed on two replicates per mixture. Displacement-control complex modulus tests are performed at 11 frequencies* (0.01, 0.1, 0.2, 0.5, 1, 2, 5, 8, 10, 20 and 30 Hz) across temperatures ranging from −20 °C to 20 °C. Stress relaxation tests are also conducted at these temperatures. A one-day recovery period is applied to verify the validity of the experimental data.

Table 3
Values of the used Δt for the complex modulus tests with different tested frequencies.

Frequency (Hz)	0.01	0.1	0.2	0.5	1	2	5	8	10	20	30
Δt (s)	1	0.1	0.05	0.02	0.01	0.005	0.002	0.001	0.001	0.0005	0.0003

Relaxation tests (Δt) = Constant 0.1s.

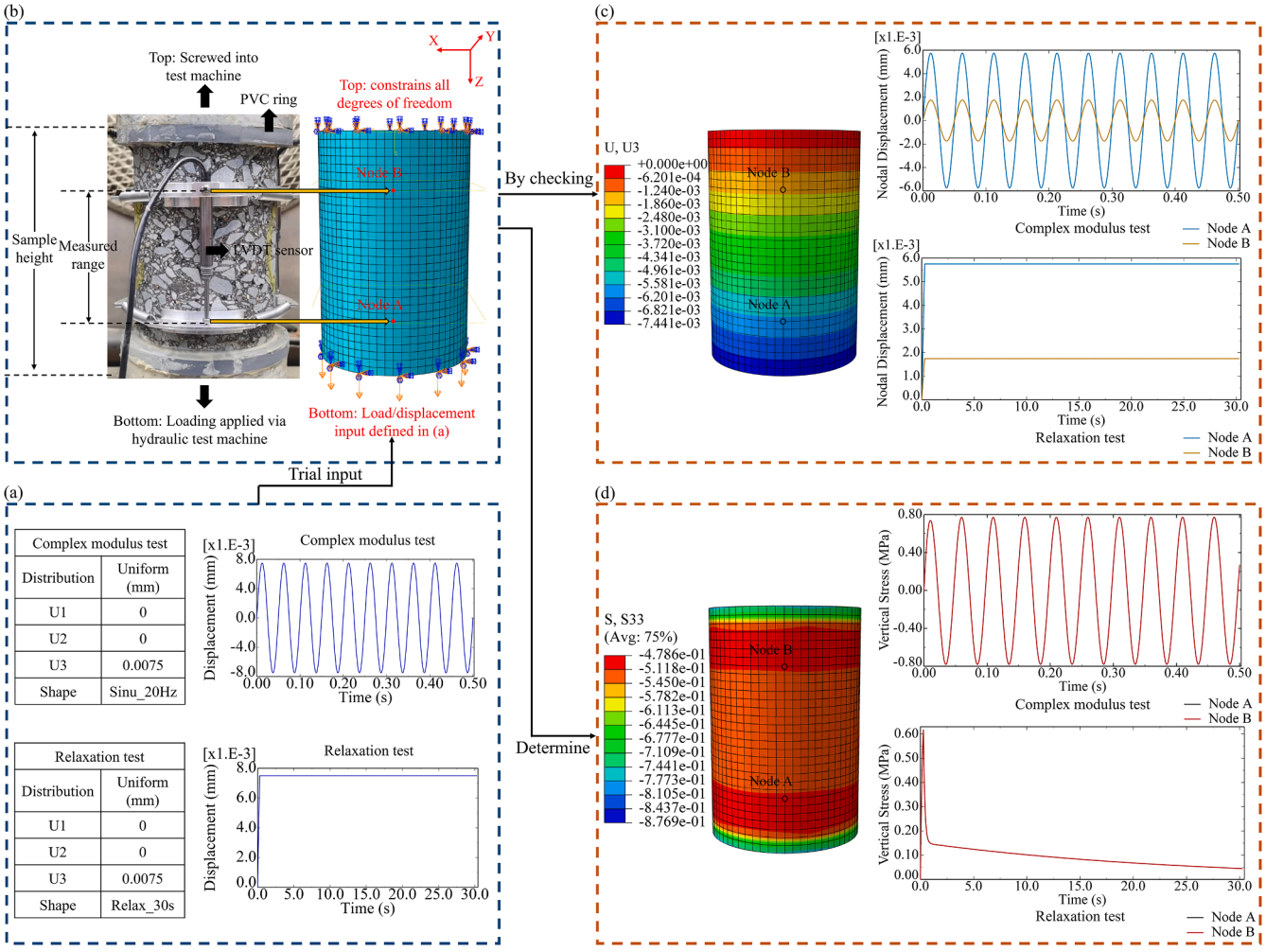

Fig. 5. FE simulation of displacement-control laboratory tests: (a) Displacement input for complex modulus test and relaxation test. U1, U2 and U3 indicate displacement levels at each input direction. "Sinu_20Hz" represents a sinusoidal waveform with a frequency of 20 Hz, while "Relax_30s" denotes a constant displacement applied for 30 s. (b) Uniaxial displacement control test setup and the FE model. In this subfigure, the three-dimensional FE model is developed based on sample geometry, with boundary conditions that reflect testing specifications. Load inputs are applied at the bottom, and stress output is recorded at two nodes (A and B) corresponding to the positions of the LVDT sensors. (c) Trial-error approach for FE nodal displacement. This iterative process is necessary because the actual displacement at the bottom boundary is unknown. Trial displacements are applied at bottom until the simulated displacements align with experimental data at the prescribed location of the LVDT. (d) FE vertical stress output from both complex modulus test and relaxation test for performance evaluation. These FE simulation results are compared with the corresponding test results.

within the proposed framework. The following subsections provide a brief description of the developed FE model used to simulate the uniaxial test setup.

4.1. Description of finite element modeling of the conducted laboratory experiments

A three-dimensional FE model was developed to simulate the laboratory tests as described in Section 3.3. In the FE model the top surface was constrained for all degrees of freedom, while the load was applied by defining the boundary condition at the bottom surface, which is similar to the operating condition of the device. For ease of understanding, corresponding loading and boundary conditions are shown in Fig. 5(a). The meshes displayed in Fig. 5(b) represents the actual mesh size adopted in the finite element simulation, which was determined based on a mesh sensitivity analysis. In the uniaxial test setup, the displacement was controlled by LVDT and the actual displacement of the bottom boundary remained unknown, which is a necessary input for the FE model. In order to solve this issue, a trial-error approach was followed in which trial displacements were applied until the simulated displacements matched with the experimental data at the prescribed location of the LVDT, as shown in Fig. 5(c). Finally, Fig. 5(d) shows a sample result of the FE simulation ($\sigma_C(t)$ and $\sigma_R(t)$) for complex modulus tests and relaxation tests. FE simulated vertical stress $\sigma_C(t)$ is used to provide the observation (see Section 5.3) to check the designed FEM model, whereas the simulated relaxation test data $\sigma_R(t)$ plays the role of

assessing the capability of Burger's model to capture the long-term behavior (see Section 5.4) under the imposed strain condition.

4.2. Implementation of the material subroutine for Burger's model

Three steps were followed to develop the material subroutine of Burger's model: a) Formulation of the time-incremental constitutive equations of Burger's model in 1D; b) 3D generalization; c) Verification of Burger's model subroutine. The following subsections are used to describe these three steps.

4.2.1. Time-incremental 1D constitutive equation of Burger's model

In this research, a recursive integral was utilized to formulate the time-incremental constitutive equations for the viscoelastic material, enabling the consideration of stress and strain history during previous loading cycle with the assumption that the Poisson ratio remains constant following past studies [88]. Keeping the above assumption in mind, the derivation of the time-incremental stress-strain relationship of Burger's model is given below.

Burger's model consists of a Maxwell element and a Kelvin-Voigt element in series. Consequently, the total strain can be expressed as the sum of three additive components, the stress remains the same for each component:

$$\varepsilon^{tot} = \varepsilon^{e} + \varepsilon^{v} + \varepsilon^{ve}, \tag{17}$$

$$\sigma = \sigma^{e} = \sigma^{v} = \sigma^{ve}, \tag{18}$$

where ε^{tot} represents the total strain, ε^{e} indicates the strain of the linear spring, ε^{v} is the strain of the linear dashpot and ε^{ve} is the strain of the Kelvin-Voigt element.

Expressing Eq. (17) in the incremental formulation yields Eq. (19):

$$\Delta\varepsilon^{tot} = \Delta\varepsilon^{e} + \Delta\varepsilon^{v} + \Delta\varepsilon^{ve}. \tag{19}$$

Each strain component in Eq. (19) can be described in terms of the incremental stress by using the compliance of each element. The detailed derivation for these strains is provided in the Supplementary material (see Section A3.1). A summary of the derivation results is presented below. For the linear spring:

$$\Delta\varepsilon^{e} = \frac{1}{E_m}\Delta\sigma(t). \tag{20}$$

For the linear dashpot:

$$\Delta\varepsilon^{v}(t) = \frac{\Delta t}{\eta_m}\left[\frac{\Delta\sigma(t)}{2} + \sigma(t-\Delta t)\right], \tag{21}$$

where the value of ε^{v} depends on the stress value at the previous time step, $\sigma(t\text{-}\Delta t)$, reflecting the hereditary (time-dependent) effect of the dashpot.

Regarding the Kelvin-Voigt element:

$$\Delta\varepsilon^{ve}(t) = \Delta\varepsilon^{ins}(t) - \Delta H(t), \tag{22}$$

where $\varepsilon^{ins}(t)$ denotes the instantaneous response in the Kelvin-Voigt element and $H(t)$ represents the recursive strain response, accounting for the hereditary effect of the Kelvin-Voigt element. The incremental form of $\varepsilon^{ins}(t)$ was described by Eq. (23):

$$\Delta\varepsilon^{ins}(t) = \frac{1}{E_k}\Delta\sigma(t). \tag{23}$$

The incremental form of $H(t)$ was derived as follows:

$$\Delta H(t) = D\cdot\left(1 - e^{-\frac{\Delta t}{\rho}}\right)\Delta\sigma(t) - \left(1 - e^{-\frac{\Delta t}{\rho}}\right)\cdot H(t-\Delta t), \tag{24}$$

where $D = \frac{\rho}{E_k\Delta t}$, represents the time-dependent compliance for the strain component of $H(t)$.

By substituting Eq. (20), Eq. (21) and Eq. (22) into the Eq. (19), the incremental form of the stress-strain relationship for Burger's model can be described by:

$$\Delta\varepsilon(t) = \left[\frac{1}{E_m} + \frac{1}{E_k} + \frac{1}{2\eta_m}\Delta t - \frac{\rho}{E_k\Delta t}\left(1 - e^{-\frac{\Delta t}{\rho}}\right)\right]\cdot\Delta\sigma(t) + \frac{\Delta t}{\eta_m}\cdot\sigma(t-\Delta t) + \left(1 - e^{-\frac{\Delta t}{\rho}}\right)\cdot H(t-\Delta t). \tag{25}$$

Rewriting Eq. (25) to express the stress function in terms of strain yields Eq. (26):

$$\Delta\sigma(t) = E\cdot\left[\Delta\varepsilon(t) - \frac{\Delta t}{\eta_m}\cdot\sigma(t-\Delta t) - \left(1 - e^{-\frac{\Delta t}{\rho}}\right)\cdot H(t-\Delta t)\right], \tag{26}$$

where $E = \frac{\partial\Delta\sigma}{\partial\Delta\varepsilon} = \frac{1}{\frac{1}{E_m}+\frac{1}{E_k}+\frac{1}{2\eta_m}\Delta t - \frac{\rho}{E_k\Delta t}\left(1 - e^{-\frac{\Delta t}{\rho}}\right)}$, represents the time-dependent modulus of the material that allows for the computation of incremental stress based on the inputs of incremental time and incremental strain.

4.2.2. Time-incremental 3D constitutive equations for Burger's model

It was found that Eq. (26) is inherently recursive and also includes the strain component $H(t)$, which updates recursively (as shown in Eq. (24)). To ensure accurate stress updates, both equations must be scripted within the subroutine algorithm which requires their formulation in three dimensions. To generalize the 1D constitutive equations into 3D equations, two matrices $\underset{\approx}{M}$ and $\underset{\approx}{N}$ were used. Matrix $\underset{\approx}{M}$ converted all the 1D modulus E into 3D modulus $\underset{\approx}{E}$, as shown in Eq. (27):

$$E \rightarrow \underset{\approx}{E} = E\cdot\underset{\approx}{M} = \frac{E}{(1+\nu)(1-2\nu)}\cdot\begin{bmatrix} 1-\nu & \nu & \nu & 0 & 0 & 0 \\ \nu & 1-\nu & \nu & 0 & 0 & 0 \\ \nu & \nu & 1-\nu & 0 & 0 & 0 \\ 0 & 0 & 0 & \frac{1-2\nu}{2} & 0 & 0 \\ 0 & 0 & 0 & 0 & \frac{1-2\nu}{2} & 0 \\ 0 & 0 & 0 & 0 & 0 & \frac{1-2\nu}{2} \end{bmatrix}, \tag{27}$$

where ν represents the Poisson's ratio. The derivation for the generalized matrix $\underset{\approx}{M}$ is provided in the Supplementary material (see Section A3.2).

Through the transformation of Eq. (27), Eq. (26) was rewritten in a 3D formulation:

$$\Delta\underset{\sim}{\sigma}(t) = \underset{\approx}{E}\cdot\Delta\underset{\sim}{\varepsilon}(t) - E\cdot\frac{\Delta t}{\eta_m}\cdot\sigma(t-\Delta t) - \underset{\approx}{E}\cdot\left(1 - e^{-\frac{\Delta t}{\rho}}\right)\cdot\underset{\sim}{H}(t-\Delta t). \tag{28}$$

It is noted that in Eq. (26), $E\cdot\frac{\Delta t}{\eta_m}$ is a dimensionless value (not a modulus). Therefore, it maintains its original form through the 3D generalization process.

Similarly, the matrix $\underset{\approx}{N}$ was used to convert the 1D compliance D into

3D compliance $\underset{\approx}{D}$ for the $H(t)$, as shown in Eq. (29):

$$D \rightarrow \underset{\approx}{D} = D \cdot \underset{\approx}{N} = D \cdot \begin{bmatrix} 1 & -\nu & -\nu & 0 & 0 & 0 \\ -\nu & 1 & -\nu & 0 & 0 & 0 \\ -\nu & -\nu & 1 & 0 & 0 & 0 \\ 0 & 0 & 0 & 2(1+\nu) & 0 & 0 \\ 0 & 0 & 0 & 0 & 2(1+\nu) & 0 \\ 0 & 0 & 0 & 0 & 0 & 2(1+\nu) \end{bmatrix}. \tag{29}$$

The derivation for the generalized matrix $\underset{\approx}{N}$ is also provided in Section A3.2 of the Supplementary material.

As a result, Eq. (24) was formulated into its 3D version:

$$\Delta \underset{\sim}{H}(t) = \left(1 - e^{-\frac{\Delta t}{\rho}}\right) \cdot \underset{\approx}{D}\, \Delta \underset{\sim}{\sigma}(t) - \left(1 - e^{-\frac{\Delta t}{\rho}}\right) \cdot \underset{\sim}{H}(t - \Delta t). \tag{30}$$

Eq. (28) and Eq. (30) represent the 3D functions of Burger's model, which can be adopted to simulate the material behavior. In this study, these 3D formulations were implemented into the commercially available finite element platform, Abaqus. A User Material (UMAT) subroutine code was scripted in FORTRAN, with the corresponding algorithm detailed in Section A3.3 of the Supplementary material.

4.2.3. *Verification of the developed material subroutine*

A verification study was conducted to demonstrate the applicability of the developed UMAT code, by assessing the FE model simulations in Abaqus. As shown in Fig. 6(a), simulations were performed on a designed cubical test block. To replicate the laboratory setup where the top of the asphalt mixture sample is mounted in the hydraulic test machine, the top of the block was fixed with constrained displacements and rotations. Meanwhile, a load was applied from the bottom. As illustrated in Fig. 6(b), the pulse load was used to simulate the typical time-dependent behavior in uniaxial load-controlled test with a recovery period.

The capability of the UMAT code is demonstrated by comparing the strain responses calculated using the analytical formulation of Burger's model (See Eq. (6)) with the results from the FE simulations. As discussed earlier, Burger's model consists of elastic, viscous and viscoelastic responses. Thus, this verification study includes a comparison for the strain responses for each component as well as the total strain response. These results have been presented in Fig. 6(c)-(f). It was found that the FE simulations closely match the analytical results with an average coefficient of determination (R^2) of 0.9910 across all comparisons. However, minor deviations are observed, particularly in Fig. 6(c) and 6(d). These deviations are likely due to the difference in dimensionality. It is apparent that the FE simulations are based on a 3D numerical solution, while the analytical results derive from a 1D equation. Despite these deviations, which are independent of the UMAT subroutine's algorithm, the results sufficiently demonstrate the applicability of the finite element model.

5. Results and discussions

Burger's model and Prony series model are the widely adopted choices for simulating the LVE behavior of asphalt mixtures, in the discrete and finite simulations. As highlighted by previous researchers, one of the challenges for using Burger's model is to find out a critical range of frequency in which its parameters could be back-calculated, so that the viscoelastic response of the material is accurately captured. In contrast, the Prony series (GM) model offers the advantage of not requiring additional frequency optimization techniques to better represent LVE behavior. However, more accurate LVE representation

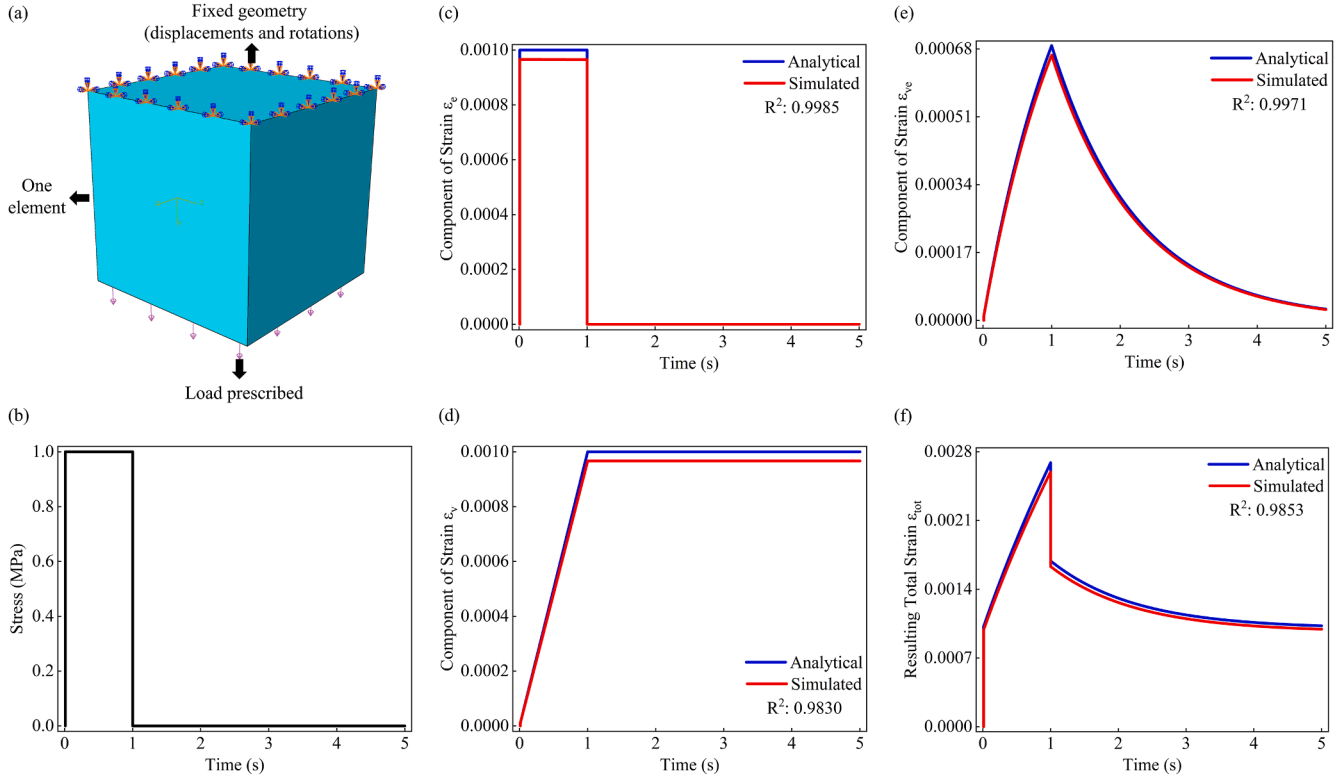

Fig. 6. Verification of the UMAT subroutine: (a) Cubical test block with defined boundary conditions. (b) Applied pulse load, which consists of one second of creep followed by four seconds of recovery. The analytical strains were compared with the FE simulated strains for each strain component: (c) elastic strain ε_e, (d) viscous strain ε_v, (e) viscoelastic ε_{ve} and (f) the total strain ε_{tot}. Note the input parameters for the verification study: σ_0=1 [MPa], E_m=1000 [Mpa], η_m=1000 [Mpa•s], E_k=800 [MPa], η_k=1000 [Mpa•s] and ν=0.3.

may require a high number of Maxwell chains. Including a high number of chains may lead to additional computational time and necessitate more data points to avoid underfitting. Although for simpler geometrical cases computation time may not be a big issue, it poses significant hurdles in the complex model. To solve these issues, this research proposes a novel statistics-based framework to automatically obtain the critical range of frequency in which accurate parameters for Burger's model could be back-calculated. Then the performance of the obtained Burger's model parameter is evaluated against the GM model in both frequency and time domains. The performance of GM model with different number of Maxwell chains is assessed in this analysis. In addition, the FE simulations of the relaxation test is used to further assess the capability of Burger's model to capture the long-term behavior (under imposed strain condition) of the examined AC mixtures. The following subsections discuss the findings in line with the above-mentioned aspects.

5.1. Determination of an optimal frequency range for the tested samples

With the described approach in the previous section (see Table 1), the parameters (E_m^i, η_m^i, E_k^i and η_k^i) of Burger's model were back-calculated for all the tested samples considering the generated frequency ranges Fi. Using the three commonly used statistical indicators (SEE, RMSE and MNE) as described in Section 2.2.2, the errors between the Tested parameters against the Reference parameters (E_m^R, η_m^R, E_k^R and η_k^R) were calculated. As shown in Fig. 7, the reduction in the data points from F1 to F9 did not provide linearly increasing/decreasing trends in errors. This observation is in line with the finding from the previous research [75–77] which postulated that a critical frequency range exists in which Burger's model seems to fit well. It could be explained by the fact that beyond the critical frequency range Burger model is not able to truly capture the nonlinearity in the material behavior.

Fig. 7(a) and Fig. 7(b) show that statistical indicators (SEE, RMSE and MNE) of F6 (0.1–20 Hz, see Table 1) is the optimal choice for the tested samples (both mixture S1 and S2). It is apparent that considering full frequency range values yields higher errors, at the same time considering frequency ranges with fewer values also results in high errors. The observation is logical that by considering only a few frequency values, meaningful information is discarded. Since the proposed statistical approach is able to identify the above over-fitting or under-fitting issues, an optimal frequency range for Burger's model is obtained.

5.2. Performance of the proposed framework with the frequency domain data

Using the approach presented in the previous subsection, an optimal frequency range (i.e., F6) was identified, and the corresponding Burger's model parameters were obtained through the adopted back-calculation approach. A detailed procedure of this approach is presented in the Supplementary material (see Section A4). To assess the improvement in prediction accuracy using the proposed framework, the master curve of Burger's model calibrated by the optimal frequency F6 was compared with that using the tested frequency range F1. Furthermore, to evaluate the characterized LVE behavior with Burger's model, the LVE characterization results from the GM model with different numbers of Maxwell chains were presented. Therefore, the effect of the different number of Maxwell chains was also discussed in this section. It is noted that in this article, the GM model was characterized using the full frequency range F1. There might be concerns that using different frequency ranges could also affect the LVE response of the GM model, although it has been demonstrated that the GM model is minimally influenced by frequency range. To clarify this, an analysis of frequency effect on the GM model was included in the Supplementary material (see Section A5), which compares the master curve calibrated by GM model using the full frequency range F1 and the frequency range F6. The results confirm that the frequency effect is negligible for the GM model. Therefore, this section focuses on the effect of frequency range on Burger's model and the effect of the number of Maxwell chains on the GM model.

A goodness-of-fit statistic was used to evaluate the fitting of the master curve. Typically, the goodness-of-fit metrics, including both the error-deviation ratio (S_e/S_y) and coefficient of determination (R^2), are calculated for the evaluation. However, due to the inclusion of the number of independent variables k (number of model parameters) in the S_e/S_y, as shown in Eq. (31), S_e/S_y becomes a more suitable indicator for the case of this study. This is because each model (Burger's model and GM model with different number of Maxwell chains in parallel) studied in this paper possesses a different number of parameters.

$$S_e = \sqrt{\frac{\sum \left(x_{\text{measured}} - x_{\text{predicted}}\right)^2}{n-k}}, \tag{31}$$

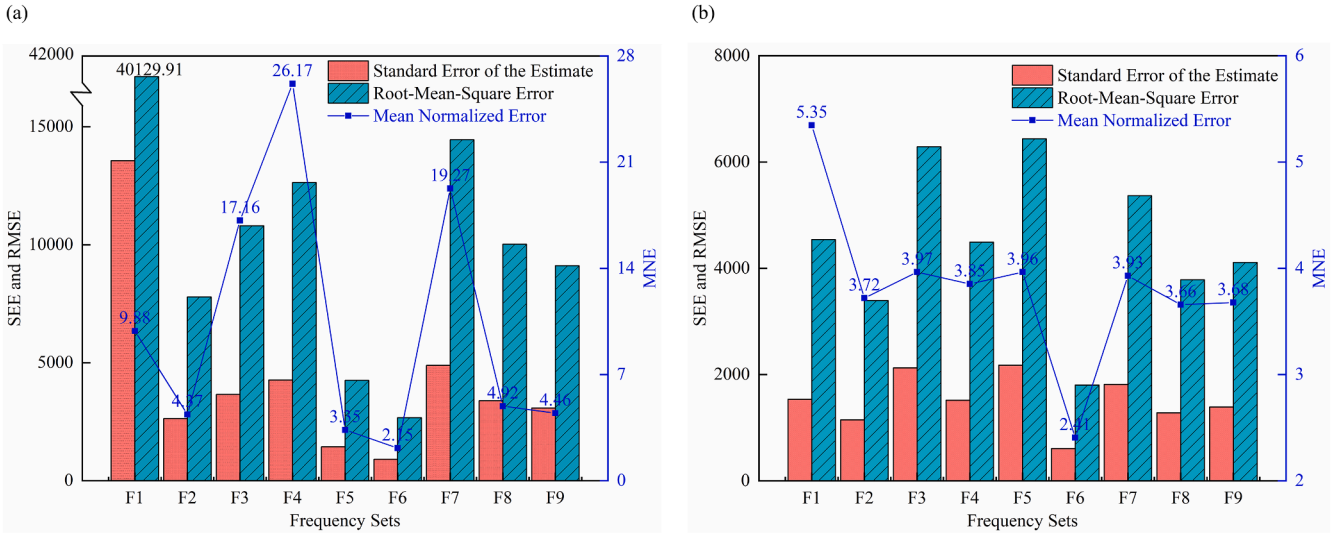

Fig. 7. Statistical analysis of Tested Parameters from different subset frequency ranges for two mixtures: (a) Mixture S1, and (b) Mixture S2. Frequency sets F1 to F9 correspond to the defined subset frequency ranges as shown in Table 1. Deviations between the model parameters obtained from different subset frequency ranges (Tested parameters) and the model parameters derived from the relaxation test data (Reference parameters) are assessed using three "statistical errors". The Standard Error of the Estimate (SEE) and Root-Mean-Square Error (RMSE) are presented in the bar chart, while the Mean Normalized Error is illustrated in the line chart. Overall, this figure demonstrates that F6 yields the lowest statistical error for both asphalt mixtures examined.

$$S_y = \sqrt{\frac{\sum (x_{\text{measured}} - \bar{x})^2}{n-1}}, \tag{32}$$

where n is the number of the measured data points, k is the number of independent variables, x_{measured} is the X data measured from the raw experimental data, $x_{\text{predicted}}$ is the X data described/predicted by the model. It is noted that in this paper, X specifically represents the dynamic modulus $|E| = \sqrt{(E')^2 + (E'')^2}$. $\bar{x}$ is the mean value of the X data. A smaller value of S_e/S_y indicates a better correlation between the measured and predicted data.

As shown in Fig. 8(a) and (b), plot B (using frequency range F6) lies closer to the pre-smoothing 2S2P1D plot as compared to plot A (using frequency range F1) for both S1 and S2 mixtures, suggesting that with the proposed optimal frequency range, better fitting can be obtained, although the typical "waveform" remains visible. Statistical investigations of these plots (see Table 4) show that the goodness-of-fit (S_e/S_y) is 0.538 for plot A and 0.358 (almost excellent level) for plot B for Mixture S1, similarly for mixture S2, 0.444 for plot A and 0.371 for plot B. Keeping S_e/S_y values of 2S2P1D 0.225 and 0.141 for Mixture S1 and S2 respectively as the best alternate fitting, it can be seen that the Burger's model in optimal frequency provides closer approximation against its full frequency range counterpart.

To have a direct comparison of the back-calculated parameters from the GM models with different number of Maxwell chains, Fig. 8(c) and (d) were plotted. It is apparent that moving from GM (2) to the GM with a greater number of Maxwell chains provides better curve fitting. This can be attributed to the fact that GM model with more Maxwell chains produces less curve waves. It is also evident in Table 4 that when the number of Maxwell chains rises from 2 to 13, the fitting improves from being statistically "Poor" to "Excellent". To ensure an "Excellent" fit of the master curve using the GM model, a minimum of four Maxwell

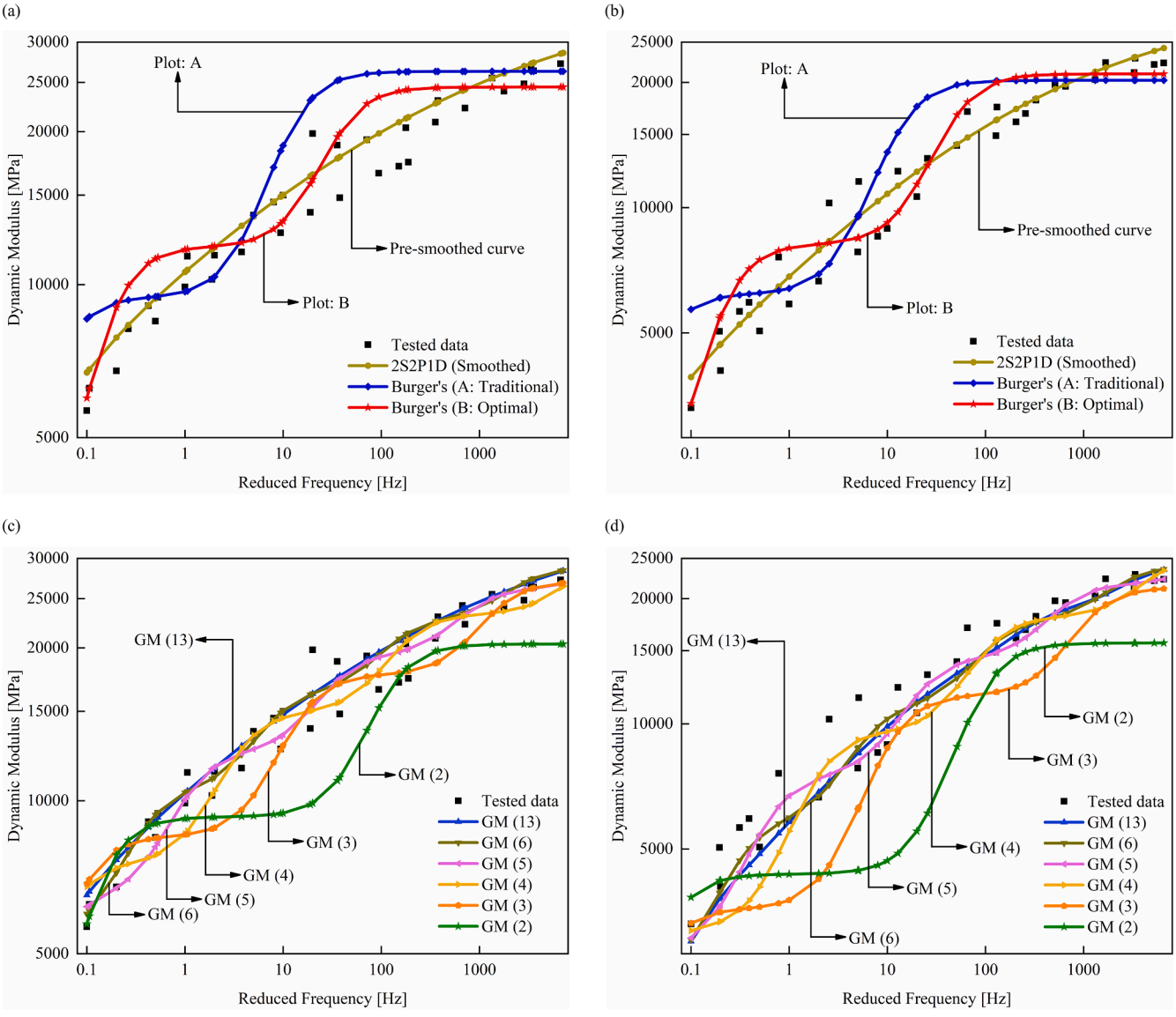

Fig. 8. Fitting of the master curve at the reference temperature of 10 °C using different models: (a) Burger's model calibrated using the complex modulus data of frequency range F1 and F6, presented with the experimental data and smoothed data from the 2S2P1D model for Mixture S1. (b) Burger's model calibrated using the complex modulus data of frequency range F1 and F6, presented with the experimental data and smoothed data from the 2S2P1D model for Mixture S2. (c) GM model with different numbers (2, 3, 4, 5, 6 and 13) of Maxwell chains calibrated using the complex modulus data of frequency range F1, presented with the experimental data for Mixture S1. (d) GM model with different numbers (2, 3, 4, 5, 6 and 13) of Maxwell chains calibrated using the complex modulus data of frequency range F1, presented with the experimental data for Mixture S2. It is noted that for the GM model, results obtained using data of F6 is presented in the Supplementary material (see Section A5).

Table 4
Evaluation for the fitting of master curve based on Goodness-of-fit statistic.

Dynamic modulus_ Mixture S1			Dynamic modulus_ Mixture S2		
Model	S_e/S_y	Classification	Model	S_e/S_y	Classification
Pre-smoothing					
2S2P1D	0.225	Excellent	2S2P1D	0.141	Excellent
Burger's model (using the full frequency range F1)					
Burger's	0.538	Good	Burger's	0.444	Good
Burger's model (using the optimal frequency range F6[1])					
Burger's	0.358	Good	Burger's	0.371	Good
GM model					
GM (13)	0.039	Excellent	GM (13)	0.164	Excellent
GM (6)	0.059	Excellent	GM (6)	0.112	Excellent
GM (5)	0.136	Excellent	GM (5)	0.141	Excellent
GM (4)	0.193	Excellent	GM (4)	0.195	Excellent
GM (3)	0.369	Good	GM (3)	0.450	Fair
GM (2)	0.671	Fair	GM (2)	0.761	Poor

(According to the Statistic Goodness-of-Fit criterion, the S_e/S_y value which is smaller than 0.35 is classified as "Excellent" curve fitting, the S_e/S_y value between 0.36 and 0.55 is classified as "Good" curve fitting, the S_e/S_y value between 0.56 and 0.75 is classified as "Fair" curve fitting, the S_e/S_y value between 0.76 and 0.89 is classified as "Poor" curve fitting, and the S_e/S_y value which is greater than 0.90 is classified as "Very poor" curve fitting [89]).

[1] Only reduced frequencies, shifted by the frequencies in this range (F6), are adopted in the statistics.

chains (nine model parameters) is required. However, it was also found that increasing the model complexity beyond GM (4) with nine parameters to GM (13) with 27 parameters results in only minimal statistical improvement, as the reduction in S_e/S_y is less than 0.2 for both mixtures. This observation reveals that there might not be much benefit of adding a greater number of Maxwell chains beyond a critical limit, with the obvious danger of statistical underfitting with artificially inflated statistical values if the number of data points is not sufficient. Nevertheless, the overall results indicate that Burger's model can achieve an almost "Excellent" condition with just four model parameters, whereas the GM model requires at least four Maxwell chains (nine parameters) and potentially increases computational time. The following section explores this aspect in greater detail.

5.3. Observations through the finite element implementation

Using the constitutive equations and material subroutine, a finite element model was developed to simulate both types of laboratory tests using Burger's model. Complex modulus values were obtained at an arbitrarily selected reference temperature (T_0=10 °C) and frequency (1Hz).

The experimental and simulated data (see Fig. 5(d)) of the initial five time periods (equivalent to five seconds for the 1 Hz test) were ignored and the subsequent data from the following four periods were utilized for further analysis. With the chosen Δt (see Table 3) for the 1 Hz test and a consistent value for the incremental time in the FE simulation, four hundred simulated data points were obtained for a detailed investigation. As shown in Fig. 9, the obtained FE simulation using different models was plotted against the laboratory-measured stress $\sigma_C(t)$, along with the line of equality [90], which indicates the FE simulated stress and the experimental stress are exactly the same. The corresponding run time (CPU time) to complete these FE simulations for different models is presented in Table 5. By adopting the FE mesh as presented in Fig. 5, the designed simulations involved a total of 12,420 C3D8H elements. All simulations were performed on a desktop PC with an i5–10210 U processor.

As shown in Fig. 9, for both mixtures S1 and S2, the FE simulated stress from Burger's model matched well with the laboratory-measured stress, with slight deviations. This could not be avoided because of the inherent waveforms as observed in the four-parameter model. In comparing Burger's model with the GM model, it can be seen that the performance of the GM model, particularly with higher number of Maxwell chains (see Fig. 9(b) and Fig. 9(d)), is closer to the equality line. Burger's model (with four parameters) performs better than the GM (2) and GM (3) model with five and seven parameters, respectively (see Fig. 9(a) and Fig. 9(c)). These results are in line with the findings in Section 5.2, which indicate that a minimum of four Maxwell chains (nine parameters) is required to ensure good quality when using Burger's model as a benchmark for evaluating the performance of GM model. The corresponding runtime data in Table 5 shows that, for the simulation of this study, Burger's model takes 27.83 % less time as compared to the GM (13). Even when considering the best GM model with lowest model parameters, GM (4) model, it still takes 22.52 % more time than Burger's model to complete the simulation. These results highlight the distinct advantage of Burger's model in reducing computational time. It is important to note that this outcome has already accounted for the additional computational cost associated with Burger's model, as the simulation of Burger's model was done via the user defined subroutines against in-built GM models.

5.4. FE-based performance evaluation of the proposed framework with the time domain data

As explained in Section 3, relaxation tests were conducted to obtain long-term material behavior under the imposed strain condition for both mixtures and FE simulations were performed with both Burger's model and GM model back-calculated parameters. The FE results of different models were plotted against the laboratory-measured stress $\sigma_R(t)$ for 120 s, as shown in Fig. 10(a) and Fig. 10(b) for both mixtures. The relaxation time was determined based on the literature [91,92] and trial tests conducted on the two asphalt mixtures.

As shown in Fig. 10, in the initial seconds, the predictions from Burger's model led to a rapid decay of the stress. This is associated with the fact that Burger's model only includes a limited number of relaxation spectrums (two relaxation times). As shown in the plots of Fig. 10(a) and Fig. 10(b), predictions from the GM model in general show a smoother transition of the decaying function whereas Burger's model exhibits a kink at around 3–4 s of the stress relaxation. Another key observation on these plots shows that in the GM model, due to its parallel arrangement and including an infinite spring element (E_∞, see Fig. 2(b)), the predicted relaxation curves approach an asymptotic non-zero value after a long-time interval, while, since all the elements in Burger's model are arranged in series (see Fig. 2(a)), the curves approach to near zero. Therefore, these results reveals that Burger's model outperforms the GM model beyond a time interval (roughly around 50 s). The inclusion of additional Maxwell chains in the GM model provides trivial improvement in predictions after this point. As mentioned in the introduction, one possible solution to address this limitation for the GM model is to add an additional dashpot in parallel with all the Maxwell chains, thereby incorporating both Maxwell and Kelvin elements. Researcher [72] have shown this modification would enhance the model's ability to more accurately describe long-term behavior. The same insight is applicable to the generalized Kelvin model with an extra dashpot connected in series with Kelvin chains as well, which can better capture the long term behavior [69–71]. However, these models are unlike the Prony series (GM) model, which are directly available in many commercial FE software packages. Furthermore, developing and analyzing these models would require significantly more effort than Burger's model.

These results demonstrate that Burger's model more accurately describes the long-term behavior of the bituminous materials studied in this paper under imposed displacement. Additional insights into predictions under imposed stress are also provided in the Supplementary material (see Section A6). As mentioned in the abstract, testing asphalt concrete and evaluating its performance over an extended service life is crucial. Several past researchers [93–95] have highlighted the importance of monitoring and simulating commonly observed distresses such

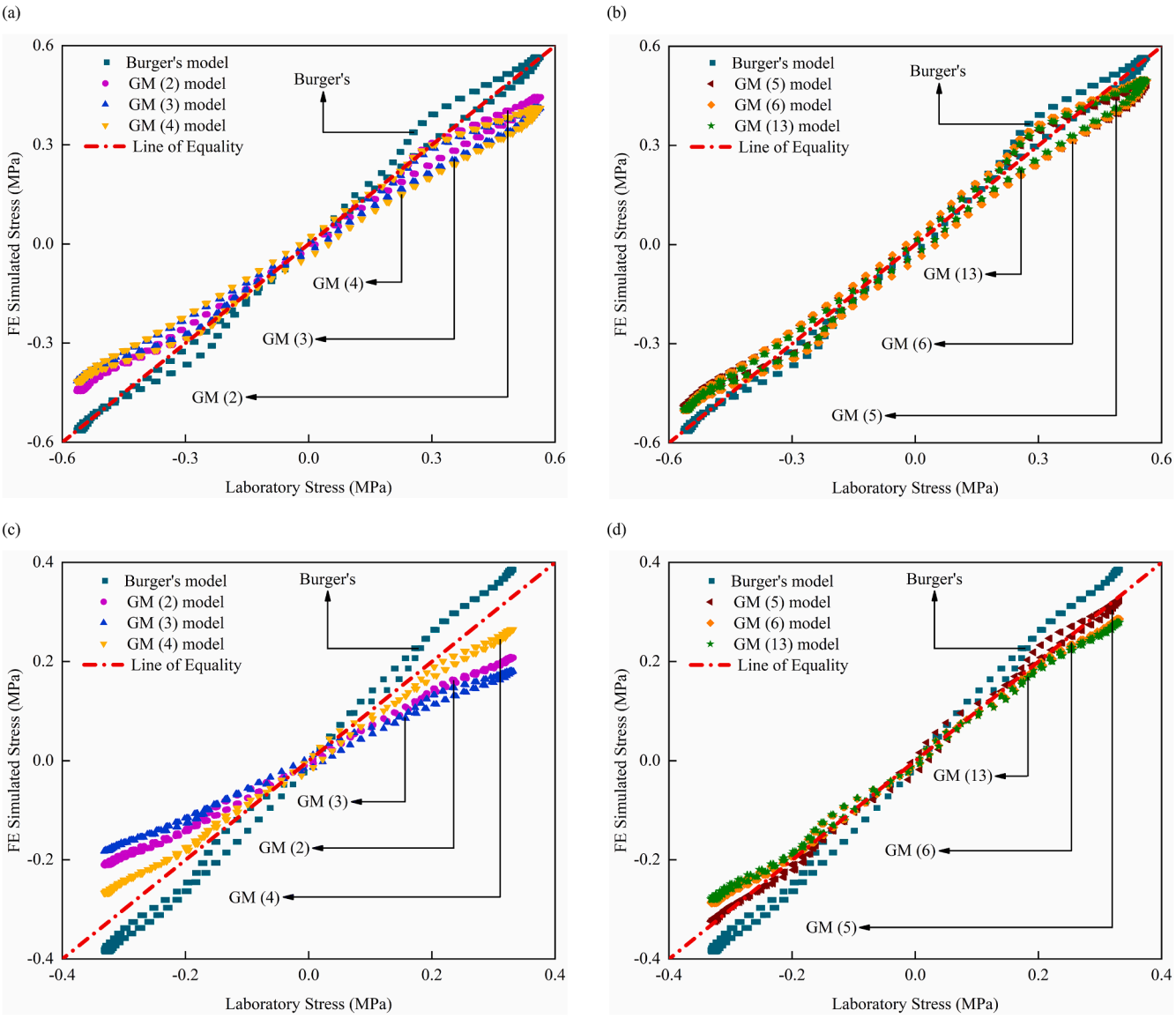

Fig. 9. FE simulated stress versus laboratory-tested stress in the complex modulus test at 10 °C and 1 Hz using different models: (a) Burger's model, presented with results from GM (2), GM (3) and GM (4) for Mixture S1. (b) Burger's model presented with results from GM (5), GM (6) and GM (13) for Mixture S1. (c) Burger's model, presented with results from GM (2), GM (3) and GM (4) for Mixture S2, (d) Burger's model, presented with results from GM (5), GM (6) and GM (13) for Mixture S2.

Table 5
CPU time.

Model	CPU time (s)
GM (13)	5991.7
GM (6)	5622.3
GM (5)	5601.9
GM (4)	5581.0
Burger's	4324.0

(Data from Mixture S1).

as fatigue, rutting and transverse cracks, which are vital for the long-term performance analysis and evaluation of asphalt pavement. In fact, prominent tests, such as the four-point bending tests, triaxial tests and indirect tensile tests (ITT), have been proposed in European [96] and American standard [97,98] to assess these aspects. Consequently, the accurate identification of the material's long-term behavior is highly valued in many studies. These results demonstrate that Burger's model is a strong choice for designing simulations in the relevant studies.

6. Conclusions

Past research has highlighted that Burger's model performs effectively within an interest range of frequencies. This presented study focuses on developing a framework for finding the critical frequency range required to obtain appropriate parameters of Burger's model. Laboratory tests, such as complex modulus tests and relaxation tests, were performed on two types of asphalt concrete mixtures. To evaluate the capability of the proposed framework, the performance of the generalized Maxwell model with different numbers of Maxwell elements was compared with Burger's model, based on both frequency domain and time domain data. Moreover, the article also presents the formulation to implement Burger's model in finite element packages. FE simulations were carried out to further evaluate the capability of Burger's model to capture the long-term behavior of the materials under imposed displacement.

The results showed that with the "optimal frequency" obtained from the proposed approach, the accuracy of the obtained Burger's model parameters has been significantly improved. For both the examined

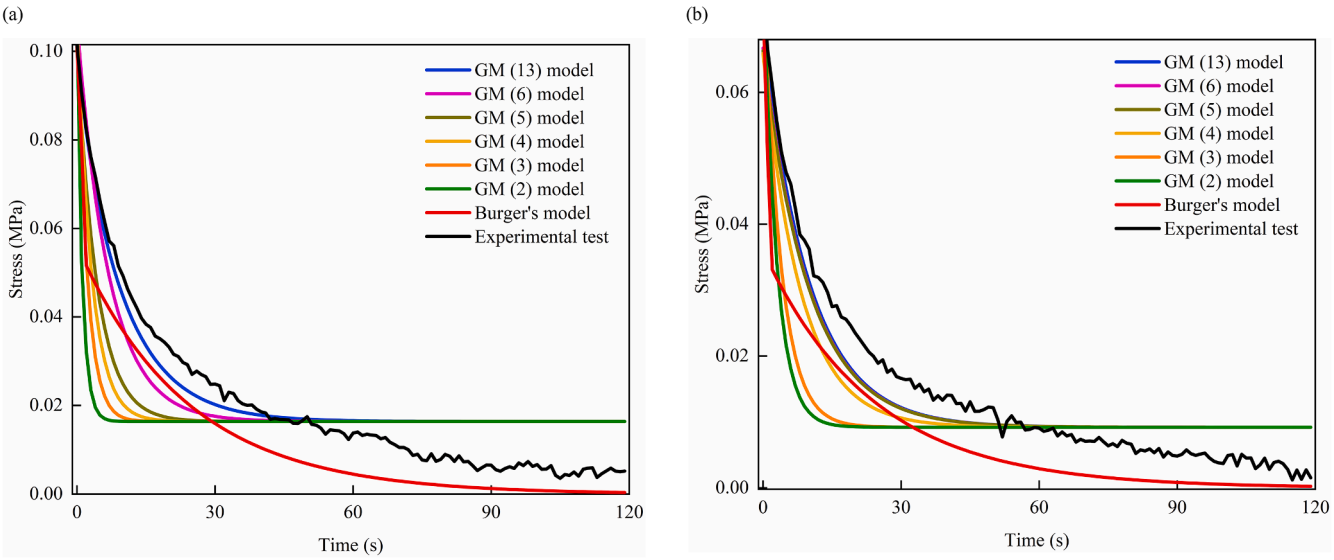

Fig. 10. FE simulated stress versus laboratory-tested stress in the relaxation test at 10 °C using Burger's model and GM model with different numbers of Maxwell chains (2, 3, 4, 5, 6 and 13): (a) Mixture S1 and (b) Mixture S2, measured up to 120 s.

mixtures, the optimal frequency range was found to be 0.1–20 Hz. This implies that both expanding and reducing the frequency range resulted in the predictions moving away from the predictions of reference parameters. This is in line with the findings of past researchers who postulated that Burger's model is applicable in a critical range of frequency. Generally, it is expected that the tested frequency range, in particular for asphalt mixtures, are broader than the identified interest range of the frequency. However, there is a concern that the optimal frequency range might fall outside the tested frequency range. Future research, which is beyond the scope of this paper, should address this issue. A promising approach could involve assessing the uncertainty of the predictions when it is beyond the tested frequency range, as results in this paper show that outside certain limit the calculated error could be significant. The magnitude of the error depends on how far the frequency deviates from the optimal range. Alternatively, one might consider using other models that remain effective across a wider frequency range instead of Burger's model.

Statistical results demonstrate that GM model requires a minimum of four Maxwell chains (nine model parameters) to maintain its good performance in accurately characterizing LVE behavior for the asphalt mixtures. These results also shows that there might not be much benefit from adding a greater number of Maxwell chains for the GM model beyond a critical limit with the obvious danger of statistical underfitting, particularly with fewer tested data points.

FE simulations of the complex modulus tests show that the performance of Burger's model was superior to the GM model with three Maxwell chains. As expected, in general, the GM model with 13 Maxwell chains produced the most accurate result but required more CPU time to complete the same FE simulation. It is noted that caution should be taken that a higher number of parameters may lead to statistical underfitting and hence unreliable results. At the same time, an ill-posed mathematical problem may also occur in the determination of the model parameters.

FE simulation for the relaxation test demonstrate that Burger's model more accurately describes the long-term behavior of the bituminous materials studied in this paper under imposed displacement. Given that accurately identifying the long-term behavior of bituminous materials is crucial for evaluating the performance of both designed and existing asphalt pavements over their extended service life, Burger's model proves to be a strong choice for designing simulations in these evaluation studies.

CRediT authorship contribution statement

Chen Wang: Writing – review & editing, Writing – original draft, Validation, Methodology, Investigation, Formal analysis, Conceptualization. **Kumar Anupam:** Writing – review & editing, Supervision, Methodology, Data curation, Conceptualization. **Cor Kasbergen:** Writing – review & editing, Supervision, Software, Formal analysis. **Sandra Erkens:** Supervision, Project administration, Data curation, Conceptualization.

Declaration of competing interest

The authors declare that they have no known competing financial interests or personal relationships that could have appeared to influence the work reported in this paper.

Acknowledgments

The first author received funding support from the China Scholarship Council (CSC, No. 201906950104) and the Dutch company Dura Vermeer is acknowledged for providing the asphalt mixture samples used in this study.

Supplementary materials

Supplementary material associated with this article can be found, in the online version, at doi:10.1016/j.ijmecsci.2024.109817.

Data availability

Data will be made available on request.

References

[1] Bauchau OA, Nemani N. Modeling viscoelastic behavior in flexible multibody systems. Multibody Syst Dyn 2021;51:159–94.
[2] Lagos-Varas M, Movilla-Quesada D, Arenas JP, Raposeiras A, Castro-Fresno D, Calzada-Pérez M, et al. Study of the mechanical behavior of asphalt mixtures using fractional rheology to model their viscoelasticity. Constr Build Mater 2019;200:124–34.
[3] Roque R, Tia M, Ruth BE. Asphalt rheology to define the properties of asphalt concrete mixtures and the performance of pavements. Asphalt rheology: relationship to mixture. ASTM International; 1987.

[4] Davis RL. Relationship between the rheological properties of asphalt and the rheological properties of mixtures and pavements. Asphalt rheology: relationship to mixture. ASTM International; 1987.
[5] Wahhab HA-A, Asi I, Ali F, Al-Dubabi I. Prediction of asphalt rheological properties using HP-GPC. J Mater Civil Eng 1999;11(1):6–14.
[6] Fernandes RR, Andrade DE, Franco AT, Negrão CO. The yielding and the linear-to-nonlinear viscoelastic transition of an elastoviscoplastic material. J Rheol (N Y N Y) 2017;61(5):893–903.
[7] Schapery RA. On the characterization of nonlinear viscoelastic materials. Polym Eng Sci 1969;9(4):295–310.
[8] Schapery RA. Nonlinear viscoelastic and viscoplastic constitutive equations based on thermodynamics. Mech Time Depend Mater 1997;1:209–40.
[9] Di Benedetto H, Partl MN, Francken L, De La Roche Saint André C. Stiffness testing for bituminous mixtures. Mater Struct 2001;34(2):66–70.
[10] Hou H, Wang T, Wu S, Xue Y, Tan R, Chen J, et al. Investigation on the pavement performance of asphalt mixture based on predicted dynamic modulus. Constr Build Mater 2016;106:11–7.
[11] Kraft M, Meissner J, Kaschta J. Linear viscoelastic characterization of polymer melts with long relaxation times. Macromolecules 1999;32(3):751–7.
[12] Agirre-Olabide I, Berasategui J, Elejabarrieta MJ, Bou-Ali MM. Characterization of the linear viscoelastic region of magnetorheological elastomers. J Intell Mater Syst Struct 2014;25(16):2074–81.
[13] Perraton D, Di Benedetto H, Sauzéat C, Hofko B, Graziani A, Nguyen QT, et al. 3Dim experimental investigation of linear viscoelastic properties of bituminous mixtures. Mater Struct 2016;49:4813–29.
[14] Odegard G, Gates T, Herring H. Characterization of viscoelastic properties of polymeric materials through nanoindentation. Exp Mech 2005;45:130–6.
[15] McKenna G, Hostetter B, Hadjichristidis N, Fetters L, Plazek D. A study of the linear viscoelastic properties of cyclic polystyrenes using creep and recovery measurements. Macromolecules 1989;22(4):1834–52.
[16] Chan RW, Rodriguez ML. A simple-shear rheometer for linear viscoelastic characterization of vocal fold tissues at phonatory frequencies. J Acoust Soc Am 2008;124(2):1207–19.
[17] Bekkour K, Kherfellah N. Linear viscoelastic behavior of bentonite-water suspensions. Appl Rheol 2002;12(5):234–40.
[18] D.-L. Chen, P.-F. Yang, Y.-S.J.M.R. Lai. A review of three-dimensional viscoelastic models with an application to viscoelasticity characterization using nanoindentation. 2012. 52(3): p. 541–58.
[19] D. Christensen Jr, T. Pellinen, R.J.J.o.t.A.o.A.P.T. Bonaquist. Hirsch model for estimating the modulus of asphalt concrete. 2003. 72.
[20] Zhang W, Chen HY, Kassab GS. A rate-insensitive linear viscoelastic model for soft tissues. Biomaterials 2007;28(24):3579–86.
[21] Sasso M, Palmieri G, Amodio D. Application of fractional derivative models in linear viscoelastic problems. Mech Time Depend Mater 2011;15:367–87.
[22] Tong S, Singh NK, Sknepnek R, Košmrlj A. Linear viscoelastic properties of the vertex model for epithelial tissues. PLoS Comput. Biol. 2022;18(5):e1010135.
[23] Park S. Analytical modeling of viscoelastic dampers for structural and vibration control. Int J Solids Struct 2001;38(44–45):8065–92.
[24] Cheng J, Qian X. Temperature-dependent viscoelastic model for asphalt concrete using discrete rheological representation. Constr Build Mater 2015;93:157–65.
[25] Shahsavari H, Naghdabadi R, Baghani M, Sohrabpour S. A viscoelastic–viscoplastic constitutive model considering damage evolution for time dependent materials: application to asphalt mixes. Int J Damage Mech 2016;25(7):921–42.
[26] Q. Xu, M.J.I.J.o.P.E. Solaimanian. Modelling linear viscoelastic properties of asphalt concrete by the Huet–Sayegh model. 2009. 10(6): p. 401–22.
[27] Chen D, Mastin N. Sigmoidal models for predicting pavement performance conditions. J Performance Construct Facilities 2016;30(4):04015078.
[28] Georgouli K, Loizos A, Plati C. Calibration of dynamic modulus predictive model. Constr Build Mater 2016;102:65–75.
[29] Unterberger MJ, Schmoller KM, Wurm C, Bausch AR, Holzapfel GA. Viscoelasticity of cross-linked actin networks: experimental tests, mechanical modeling and finite-element analysis. Acta Biomater 2013;9(7):7343–53.
[30] Thamburaja P, Ekambaram R. Coupled thermo-mechanical modelling of bulk-metallic glasses: theory, finite-element simulations and experimental verification. J Mech Phys Solids 2007;55(6):1236–73.
[31] Tang T, Anupam K, Kasbergen C, Scarpas A, Erkens S. A finite element study of rain intensity on skid resistance for permeable asphalt concrete mixes. Constr Build Mater 2019;220:464–75.
[32] H. Feng, M. Pettinari, H.J.C. Stang, B. Materials. Study of normal and shear material properties for viscoelastic model of asphalt mixture by discrete element method. 2015. 98: p. 366–75.
[33] Liu Y, Dai Q, You Z. Viscoelastic model for discrete element simulation of asphalt mixtures. J Eng Mech 2009;135(4):324–33.
[34] Thakur SC, Morrissey JP, Sun J, Chen J, Ooi JY. Micromechanical analysis of cohesive granular materials using the discrete element method with an adhesive elasto-plastic contact model. Granul Matter 2014;16:383–400.
[35] Grzywacz H, Jenczyk P, Milczarek M, Michałowski M, Jarząbek DM. Burger model as the best option for modeling of viscoelastic behavior of resists for nanoimprint lithography. Materials (Basel) 2021;14(21):6639.
[36] Dey A, Basudhar PJGAiA. Modeling, design. Applicab Burger Model Predict Response Viscoelastic Soil Beds 2010:2611–20.
[37] Underwood SB, Kim RY. Viscoelastoplastic continuum damage model for asphalt concrete in tension. J Eng Mech 2011;137(11):732–9.
[38] Underwood BS, Yun T, Kim YR. Experimental investigations of the viscoelastic and damage behaviors of hot-mix asphalt in compression. J Mater Civil Eng 2011;23(4):459–66.
[39] Mottahedi M, Dadalau A, Hafla A, Verl A. Numerical analysis of relaxation test based on Prony series material model. Integrated systems, design and technology 2010: knowledge transfer in new technologies. Springer; 2011.
[40] Duffrene L, Gy R, Burlet H, Piques R. Multiaxial linear viscoelastic behavior of a soda–lime–silica glass based on a generalized Maxwell model. J Rheol (N Y N Y) 1997;41(5):1021–38.
[41] Olard F, Di Benedetto HJRm. p. design. General "2S2P1D" model and relation between the linear viscoelastic behaviours of bituminous binders and mixes 2003;4(2):185–224.
[42] Craiem D, Armentano RL. A fractional derivative model to describe arterial viscoelasticity. Biorheology 2007;44(4):251–63.
[43] Mainardi F. Fractional calculus and waves in linear viscoelasticity: an introduction to mathematical models. World Scientific; 2022.
[44] Rossikhin YA, Shitikova M. Application of fractional derivatives to the analysis of damped vibrations of viscoelastic single mass systems. Acta Mech 1997;120(1):109–25.
[45] Yusoff M, Airey G. The 2S2P1D: an excellent linear viscoelastic model. J Civil Eng Sci Technol 2010;1(2):1–7.
[46] Bonfanti A, Kaplan JL, Charras G, Kabla A. Fractional viscoelastic models for power-law materials. Soft Matter 2020;16(26):6002–20.
[47] Luo R, Lv H, Liu H. Development of Prony series models based on continuous relaxation spectrums for relaxation moduli determined using creep tests. Constr Build Mater 2018;168:758–70.
[48] Li L, Li W, Wang H, Zhao J, Wang Z, Dong M, et al. Investigation of Prony series model related asphalt mixture properties under different confining pressures. Constr Build Mater 2018;166:147–57.
[49] de Araújo PC, Soares JB, de Holanda ÁS, Parente E, Evangelista F. Dynamic viscoelastic analysis of asphalt pavements using a finite element formulation. Road Mater Pavement Des 2010;11(2):409–33.
[50] Taherkhani H, Jalali M. Investigating the performance of geosynthetic-reinforced asphaltic pavement under various axle loads using finite-element method. Road Mater Pavement Des 2017;18(5):1200–17.
[51] Kim Y-R, Little D, Lytton R. Fatigue and healing characterization of asphalt mixtures. J Mater Civil Eng 2003;15(1):75–83.
[52] Kim Y-R, Allen D, Little D. Computational constitutive model for predicting nonlinear viscoelastic damage and fracture failure of asphalt concrete mixtures. Int J Geomech 2007;7(2):102–10.
[53] Ghoreishy MHR. Determination of the parameters of the Prony series in hyper-viscoelastic material models using the finite element method. Mater Des 2012;35:791–7.
[54] Suchocki C, Molak R. On relevance of time-dependent Poisson's ratio for determination of relaxation function parameters. J Brazil Soc Mech Sci Eng 2019;41:1–14.
[55] Bharadwaj M, Claramunt S, Srinivasan S. Modeling creep relaxation of polytetrafluorethylene gaskets for finite element analysis. Int J Mater Mech Manuf 2017;5(2):123–6.
[56] Woldekidan M, Huurman M, Pronk A. Linear and nonlinear viscoelastic analysis of bituminous mortar. Transp Res Rec 2013;2370(1):53–62.
[57] Xu X, Gupta N. Application of radial basis neural network to transform viscoelastic to elastic properties for materials with multiple thermal transitions. J Mater Sci 2019;54(11):8401–13.
[58] Jalocha D, Constantinescu A, Neviere R. Revisiting the identification of generalized Maxwell models from experimental results. Int J Solids Struct 2015;67:169–81.
[59] Srirangam S, Anupam K, Scarpas A, Kasbergen C. Development of a thermomechanical tyre–pavement interaction model. Int J Pavement Eng 2015;16(8):721–9.
[60] G. Dondi, V. Vignali, M. Pettinari, F. Mazzotta, A. Simone, C.J.C. Sangiorgi, et al. Modeling the DSR complex shear modulus of asphalt binder using 3D discrete element approach. 2014. 54: p. 236–46.
[61] J.J.I.J.o.P.E. Judycki. A new viscoelastic method of calculation of low-temperature thermal stresses in asphalt layers of pavements. 2018. 19(1): p. 24–36.
[62] Razavi SM, Taheri H, Sanchez R. Viscoelastic characterization of sage seed gum. Int J Food Properties 2013;16(7):1604–19.
[63] Dey A, Basudhar PK. Parameter estimation of four-parameter viscoelastic Burger model by inverse analysis: case studies of four oil-refineries. Interaction and multiscale mechanics 2012;5(3):211–28.
[64] Duffy JJ, Rega CA, Jack R, Amin S. An algebraic approach for determining viscoelastic moduli from creep compliance through application of the Generalised Stokes-Einstein relation and Burgers model. Appl Rheol 2016;26(1):10–5.
[65] G.C. Papanicolaou, G.P. Lagas, S.P.J.J.o.A.P.S. Zaoutsos. Viscoelastic behavior of hybrid building materials. 2015. 132(6).
[66] Vu AT, Vu AN, Grunwald T, Bergs T. Modeling of thermo-viscoelastic material behavior of glass over a wide temperature range in glass compression molding. Journal of the American Ceramic Society 2020;103(4):2791–807.
[67] Ma T, Wang H, Zhang D, Zhang Y. Heterogeneity effect of mechanical property on creep behavior of asphalt mixture based on micromechanical modeling and virtual creep test. Mechanics of Materials 2017;104:49–59.
[68] Wan P, Liu Q, Wu S, Zhao Z, Chen S, Zou Y, et al. A novel microwave induced oil release pattern of calcium alginate/nano-Fe3O4 composite capsules for asphalt self-healing. J Clean Prod 2021;297:126721.
[69] A.C. Collop, A. Scarpas, C. Kasbergen, A.J.T.R.R. de Bondt. Development and finite element implementation of stress-dependent elastoviscoplastic constitutive model with damage for asphalt. 2003. 1832(1): p. 96–104.
[70] Ren J, Liu Z, Xue J, Xu Y. Influence of the mesoscopic viscoelastic contact model on characterizing the rheological behavior of asphalt concrete in the DEM simulation. Advances in civil engineering 2020;2020(1):5248267.

[71] Câmara G, Azevedo NM, Micaelo R, Silva H. Generalised Kelvin contact models for DEM modelling of asphalt mixtures. International Journal of Pavement Engineering 2023;24(1):2179625.
[72] Ren J, Sun L. Generalized Maxwell viscoelastic contact model-based discrete element method for characterizing low-temperature properties of asphalt concrete. Journal of Materials in Civil Engineering 2016;28(2):04015122.
[73] Aberoumand M, Rahmatabadi D, Soltanmohammadi K, Soleyman E, Ghasemi I, Baniassadi M, et al. Stress recovery and stress relaxation behaviors of PVC 4D printed by FDM technology for high-performance actuation applications. Sensors and Actuators A: Physical 2023;361:114572.
[74] Nilsson RN, Hopman PC, Isacsson U. Influence of different rheological models on predicted pavement responses in flexible pavements. Road Materials and Pavement Design 2002;3(2):117–49.
[75] A.C. Pronk. The Huet-Sayegh model: a simple and excellent rheological model for master curves of asphaltic mixes, in Asphalt Concrete: Simulation, Modeling, and Experimental Characterization. 2006. p. 73–82.
[76] Hopman P. VEROAD: a viscoelastic multilayer computer program. Transp Res Rec 1996;1539(1):72–80.
[77] Mazurek G, Iwański M. Modelling of asphalt concrete stiffness in the linear viscoelastic region. In: IOP Conference Series: Materials Science and Engineering. IOP Publishing; 2017.
[78] Park S, Schapery RJIjos. structures. Methods of interconversion between linear viscoelastic material functions. Part I—A numerical method based on Prony series 1999;36(11):1653–75.
[79] Cao Y, Ma D, Raabe D. The use of flat punch indentation to determine the viscoelastic properties in the time and frequency domains of a soft layer bonded to a rigid substrate. Acta Biomater 2009;5(1):240–8.
[80] Zhang Y, Sun Y. Fast-acquiring high-quality Prony series parameters of asphalt concrete through viscoelastic continuous spectral models. Materials (Basel) 2022;15(3):716.
[81] S. Park, Y.J.J.o.m.i.c.e. Kim. Fitting Prony-series viscoelastic models with power-law presmoothing. 2001. 13(1): p. 26–32.
[82] Kutay ME, Chatti K, Lei L. Backcalculation of dynamic modulus mastercurve from falling weight deflectometer surface deflections. Transp Res Rec 2011;2227(1):87–96.
[83] Sun Y, Huang B, Chen J, Jia X, Ding Y. Characterizing rheological behavior of asphalt binder over a complete range of pavement service loading frequency and temperature. Constr Build Mater 2016;123:661–72.
[84] Sun Y, Huang B, Chen J. A unified procedure for rapidly determining asphalt concrete discrete relaxation and retardation spectra. Constr Build Mater 2015;93:35–48.
[85] Yu D, Yu X, Gu Y. Establishment of linkages between empirical and mechanical models for asphalt mixtures through relaxation spectra determination. Constr Build Mater 2020;242:118095.
[86] Ren S, Liu X, Wang H, Fan W, Erkens S. Evaluation of rheological behaviors and anti-aging properties of recycled asphalts using low-viscosity asphalt and polymers. J Clean Prod 2020;253:120048.
[87] Juhany KA, Shahzad F, Alzhrani S, Pasha AA, Jamshed W, Islam N, et al. Finite element mechanism and quadratic regression of magnetized mixed convective Burgers' nanofluid flow with applying entropy generation along the riga surface. Int Commun Heat and Mass Transfer 2023;142:106631.
[88] Lai J, Bakker A. 3-D Schapery representation for non-linear viscoelasticity and finite element implementation. Comput Mech 1996;18(3):182–91.
[89] N.I.M. Yusoff, D. Mounier, G. Marc-Stéphane, M.R. Hainin, G.D. Airey, H.J.C. Di Benedetto, et al. Modelling the rheological properties of bituminous binders using the 2S2P1D Model. 2013. 38: p. 395–406.
[90] Bland JM, Altman DG. Applying the right statistics: analyses of measurement studies. Ultrasound in Obstetr Gynecol 2003;22(1):85–93.
[91] Si Z, Little D, Lytton R. Characterization of microdamage and healing of asphalt concrete mixtures. J Mater Civil Eng 2002;14(6):461–70.
[92] Luo X, Luo R, Lytton RL. Characterization of recovery properties of asphalt mixtures. Constr Build Mater 2013;48:610–21.
[93] Hong F, Chen D-H, Mikhail MM. Long-term performance evaluation of recycled asphalt pavement results from Texas: pavement studies category 5 sections from the long-term pavement performance program. Transp Res Rec 2010;2180(1):58–66.
[94] Sudarsanan N, Kim YR. A critical review of the fatigue life prediction of asphalt mixtures and pavements. J Traffic Transport Eng (English Edition) 2022;9(5):808–35.
[95] Norouzi A, Kim D, Kim YRichard. Numerical evaluation of pavement design parameters for the fatigue cracking and rutting performance of asphalt pavements. Mater Struct 2016;49:3619–34.
[96] Dehghan Z, Modarres A. Evaluating the fatigue properties of hot mix asphalt reinforced by recycled PET fibers using 4-point bending test. Constr Build Mater 2017;139:384–93.
[97] Roy N, Veeraragavan A, Jain P, Krishnan JM. A re-look at the asphalt mixture performance test protocols and computational algorithms. J Test Eval 2013;41(5):729–44.
[98] Li Q, Xiao DX, Wang KC, Hall KD, Qiu Y. Mechanistic-empirical pavement design guide (MEPDG): a bird's-eye view. J Modern Transport 2011;19:114–33.